Quantitative Assessment of Aerocapture and Applications to Future Solar System Exploration

Athul Pradeepkumar Girija,* Sarag J. Saikia,† and James M. Longuski‡
Purdue University, West Lafayette, Indiana 47907
Ye Lu§
Kent State University, Kent, Ohio 44242
and
James A. Cutts¶
Jet Propulsion Laboratory, California Institute of Technology, Pasadena, California 91109

https://doi.org/10.2514/1.A35214

A quantitative and comparative assessment of the feasibility and mass benefit of using aerocapture at all atmosphere-bearing solar system destinations is presented, considering both lift and drag modulation control techniques. Aerocapture is shown to be feasible at Mars, Titan, and Venus with existing entry vehicles and flight-proven thermal protection system (TPS) materials, and requires no significant technology developments before use on a science mission. Aerocapture at Uranus and Neptune is viable with blunt-body aeroshells (L/D of 0.30–0.40) and Heatshield for Extreme Entry Environment Technology TPS for certain high arrival V_∞ interplanetary trajectories. The mass benefit offered by aerocapture is compared to alternative orbit insertion techniques such as purely propulsive insertion and aerobraking. Aerobraking outperforms aerocapture for missions to Mars and Venus with arrival V_∞ less than 6 km/s. For outer planet missions, aerocapture offers substantial mass benefit depending on the arrival V_∞, Titan (300–1700% more mass), Uranus (100–600%), and Neptune (80–400%), in addition to significant reduction in flight time. The study recommends a low-cost drag modulation aerocapture demonstration mission at Earth to establish flight heritage for aerocapture and lower the risk for future science missions.

I. Introduction

AEROCAPTURE is a maneuver in which a spacecraft uses aerodynamic drag from a single atmospheric pass to decelerate and achieve orbit insertion. Compared to conventional propulsive orbit insertion, aerocapture allows interplanetary spacecraft to accomplish a near-propellantless method of capture at any planetary destination with a significant atmosphere. The overall mass savings offered by aerocapture has motivated the development of aerocapture mission concepts to every atmosphere bearing destination in the solar system over the past six decades. For inner planets such as Mars and Venus, aerocapture is an attractive technology for small satellite orbit insertion [1–3]. For outer planet missions, aerocapture can enable orbit insertion from significantly shorter-time-of-flight, fast-arrival interplanetary trajectories that are not feasible with propulsive insertion [4–6]. Several aerocapture mission concepts and technology demonstration flights have been proposed and studied over the past three decades, but an end-to-end aerocapture mission has never been flown. However, many aspects of aerocapture such as guided hypersonic flight using blunt-body aeroshells and high-performance thermal protection system (TPS) materials have been demonstrated successfully on the Mars Science Laboratory (MSL) and Apollo entry vehicles [7].

Aerocapture has been studied extensively by many authors as seen in Fig. 1, which shows a histogram of the number of publications over the past six decades. London [8] was the first to propose the use of aerodynamic forces to achieve satellite plane change for orbital vehicles. The use of aerocapture for orbit attainment at Venus and Mars has been studied since the early 1960s, though the concept was then referred to as aerobraking by Repic et al. [9] and other authors [10,11]. Till the early 1990s, the terms *aerobraking* and *aerocapture* were used interchangeably but are fundamentally different maneuvers. In aerobraking the spacecraft performs a propulsive burn on arrival to get captured into a highly elliptical orbit and subsequently uses multiple upper atmospheric passes to lower the apoapsis over the course of several weeks to a few months. The aerobraking maneuver typically requires no TPS as the velocity decrements over any one upper atmospheric pass are only a few meters per second compared to several kilometers per second for aerocapture. Cruz [12], in 1979, was the first to define the aerocapture mission concept and distinguish aerocapture from the concept of aerobraking. There was significant interest in the application of aerocapture for the Mars Sample Return (MSR) mission in the early 1980s, as well as for the Venus Orbiting Imaging Radar [13,14]. In the late 1980s, the Aeroassist Flight Experiment (AFE) was conceived to demonstrate aerocapture at Earth but was eventually canceled because of cost overruns [15]. Aerocapture was considered for the Mars Odyssey mission, but was later dropped in favor of aerobraking due to cost reasons and heritage with other Mars missions [16]. Aerocapture was also considered for the joint NASA/CNES Mars Sample Return Orbiter mission, but was canceled in the wake of the failure of the Mars Climate Orbiter and the Mars Polar Lander missions [17]. In 2001, the Aerocapture Flight Test Experiment, which proposed to demonstrate aerocapture at Earth, was one of the candidates in NASA's New Millennium Program ST-7 competition [18], and again in the ST-9 competition in 2006 [19], though both were ultimately not flown. Till the early 2000s, most of the aerocapture studies were directed at Mars, particularly sample return missions.

A large number of aerocapture-related publications appear in the early 2000s primarily attributed to a multicenter NASA effort as part

Received 23 July 2021; revision received 15 November 2021; accepted for publication 21 December 2021; published online 22 February 2022.

*Doctoral Candidate, School of Aeronautics and Astronautics; apradee@purdue.edu. Student Member AIAA.

†Research Assistant Professor, School of Aeronautics and Astronautics; currently CEO, Spacefaring Technologies Private Limited; saragjs@gmail.com.

‡Professor, School of Aeronautics and Astronautics; longuski@purdue.edu. Associate Fellow AIAA.

§Assistant Professor, College of Aeronautics and Engineering; ylu16@kent.edu.

¶Program Manager, Solar System Exploration Directorate; james.a.cutts@jpl.nasa.gov.

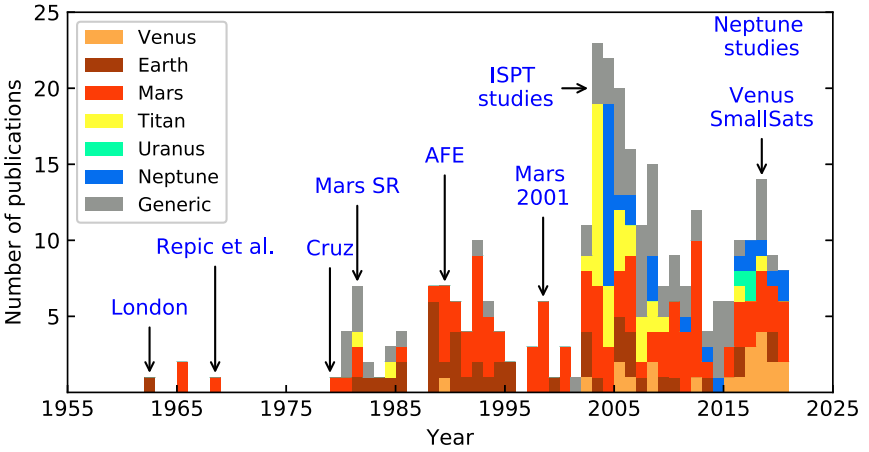

Fig. 1 Number of publications related to aerocapture over the past six decades, colored by target planet. Data available at https://github.com/athulpg007/AMAT/tree/master/bibliometric-data.

of the NASA In-Space Technology (ISPT) Program studies [20]. The studies assessed the benefits offered by aerocapture at Venus, Mars, Titan, and Neptune in comparison to purely propulsive insertion and aerobraking. The ISPT studies concluded that aerocapture offers significant increase in delivered payload mass for missions to Mars, Venus, and Titan using aerocapture, and enables entirely new class of missions to Neptune [4,21–24]. In 2005, Hall et al. [25] performed a study that showed that aerocapture could enhance missions to Venus, Mars, Titan, and Uranus and enable some missions to Jupiter, Saturn, and Neptune. The study analyzed a set of aerocapture missions to various destinations and quantified the mass benefit of aerocapture compared to propulsive insertion: Venus (79% more mass), Mars (15%), Titan (280%), Uranus (218%), and Neptune (832%) [25]. Ingersoll and Spilker [26] highlighted the importance of using aerocapture for a Neptune mission to achieve significant science within reasonable flight times. In 2012, the Japan Aerospace Exploration Agency (JAXA) performed detailed studies involving mission and spacecraft design for a low-cost Mars aerocapture demonstration mission [27]. In 2014, Putnam and Braun [28] developed drag-modulation mission concepts for planetary aerocapture, and highlighted its applications to small satellite orbit insertion at Venus, Mars, and Titan. In 2016, Saikia et al. [29] performed an assessment of aerocapture in support of the NASA Ice Giants Pre-Decadal Survey Mission Study, which identified potential high arrival V_∞ short time-of-flight interplanetary trajectories for aerocapture at Uranus and Neptune [30]. The Ice Giants Pre-Decadal mission study motivated a number of follow-on studies focusing on aerocapture at Neptune for a future Flagship-class mission [5,31,32].

In 2016, Spilker et al. [7] performed a study initiated by the NASA Planetary Science Division (PSD) to assess the readiness of aerocapture for future missions. The study concluded that an end-to-end aerocapture technology demonstration is not necessary before use on a planetary mission. The study found that existing entry system technologies and TPS materials are feasible for aerocapture missions to Venus, Mars, and Titan, and require no additional technology developments aside from engineering developments common to any space mission. Missions to Uranus and Neptune using aerocapture may require development of mid-L/D aeroshells, and the study team concluded that at least additional studies were required to evaluate the readiness of aerocapture for ice giant missions. Aerocapture at Jupiter is considered a long-term goal due to the very high entry speeds and harsh aerothermal environments far beyond the capability of existing TPS materials [7], and propulsive insertion is the preferred option for the foreseeable future. For Saturn orbit insertion, aerogravity assist at Titan is a viable method due to the less demanding aerothermal conditions [33–35].

Drag modulation aerocapture has received renewed interest with its applications to small satellites for low-cost technology demonstration and rideshare planetary science missions to Mars and Venus. Werner and Braun [36] studied a SmallSat mission architecture to demonstrate aerocapture at Earth using a geosynchronous transfer orbit rideshare trajectory. Numerous recent studies have investigated the feasibility, mission design, and guidance performance for SmallSat mission concepts leveraging drag modulation aerocapture at Mars and Venus [2,37–41]. Drag modulation aerocapture could enable small satellite constellations such as those currently operational in low Earth orbit (LEO) and could enable a new paradigm for Mars and Venus exploration within the next decade [1,42].

The study by Hall et al. [25] in 2005 remains the only study to quantitatively assess and compare aerocapture performance across the entire range of planetary destinations. One limitation of the study is that it assumed that both aerocapture and propulsive insertion architectures use the same interplanetary trajectory, which is not necessarily optimized for a particular architecture. Also, since 2005, many technology developments have occurred in the field of TPS, guidance techniques, and interplanetary SmallSats. Spilker et al. [7] performed a comprehensive review of the aerocapture technology readiness for future missions, but it remains largely qualitative.

The present study aims to perform a quantitative and comparative assessment of aerocapture across the full set of solar system targets with applications to future missions. Researchers at Purdue University have developed a framework for rapid mission design studies considering the coupled nature of interplanetary arrival conditions and vehicle performance for aerocapture [43]. Lu and Saikia [44] applied the methodology for lift modulation aerocapture at Titan considering a range of vehicle L/D and interplanetary arrival conditions. Girija et al. [3] applied the methodology for aerocapture at Venus, including both lift and drag modulation techniques. Girija et al. [5] applied the methodology for aerocapture at Neptune to identify short-time-of-flight, high-arrival-V_∞ trajectories that lower the vehicle L/D requirement from 0.6–0.8 to 0.3–0.4. This paper extends the methodology to all atmosphere-bearing solar system destinations—Venus, Earth, Mars, Jupiter, Saturn, Titan, Uranus, and Neptune. Aerocapture feasibility charts are used to concisely present the various constraints arising from corridor width, deceleration, and heating requirements for both lift and drag modulation techniques. Mission designers can quickly assess the feasibility of aerocapture for a mission concept to any atmosphere-bearing destination using a limited number of design parameters. The mass-benefit analysis enables comparison of the delivered mass with alternative orbit insertion techniques such as aerobraking and purely propulsive insertion for a range of interplanetary arrival conditions. The paper also introduces a new open-source software for rapid conceptual design of aerocapture missions, the Aerocapture Mission Analysis Tool (AMAT), whose features and capabilities are briefly discussed. AMAT can be used to quickly assess aerocapture feasibility, select a baseline architecture, as well as perform Monte Carlo simulations to assess aerocapture vehicle performance [45].

II. Methodology

Aerocapture feasibility charts use a graphical approach to visualize the various constraints arising from control authority requirement, peak deceleration, stagnation-point peak heat rate, and total heat load as a function of vehicle aerodynamic performance and interplanetary arrival conditions. The mission designer can select acceptable constraint values in the feasibility charts and define the feasible set of key vehicle performance parameters such as lift-to-drag ratio L/D (for lift modulation aerocapture) or the ballistic coefficient ratio β_2/β_1 (for drag modulation aerocapture) and the range of feasible interplanetary arrival V_∞ values. The procedure for creating the aerocapture feasibility charts and their application to trade studies have been extensively discussed in previous studies [3,5,44]. A brief discussion of the key aerocapture vehicle design considerations—theoretical corridor width, peak deceleration, peak heat rate, and total heat load used in the aerocapture feasibility charts—is given below.

A. Theoretical Corridor Width

To perform aerocapture, the entry vehicle must enter the atmosphere within the aerocapture corridor bounded by the minimum and maximum acceptable entry flight-path angles (EFPAs) as shown in Fig. 2.

The minimum EFPA $\gamma_{\min}$ (undershoot limit) is the steepest EFPA at which the vehicle can enter and achieve the desired atmospheric exit conditions to achieve the target apoapsis. The maximum EFPA $\gamma_{\max}$ (overshoot limit) is the shallowest allowable for the vehicle to achieve the desired orbit upon atmospheric exit. The difference between the two bounding EFPAs is termed the *theoretical corridor width* (TCW), and it is a measure of the vehicle control authority.

$$\mathrm{TCW} = |\gamma_{\max} - \gamma_{\min}| \tag{1}$$

The required corridor width (RCW) is a measure of the combined uncertainties in approach navigation, atmospheric density, and other uncertainties [23]. For the vehicle to perform the aerocapture maneuver without risking crashing into the planet or flyaway without getting captured, the available TCW must exceed the RCW.

$$\mathrm{TCW} \geq \mathrm{RCW} + \epsilon \tag{2}$$

where ϵ is additional margin to accommodate factors such as shallow limit sensitivity and high-frequency density perturbations [5,23]. If the available TCW exceeds the RCW with sufficient margin, vehicle control authority is deemed adequate. Calculation of the RCW requires knowledge of the delivery error, the atmospheric uncertainty, and aerodynamic uncertainties to be expected [5,23]. Typical values of RCW are expected to be in the range of 0.5–1.0 deg for Venus, Earth, Mars, and Titan, whose atmospheres are relatively well known [4,22]. For Uranus and Neptune, whose atmospheres have large uncertainties, typical RCW values are in the range of 1.0–2.0 deg [4,5]. Table 1 lists the nominal delivery errors and TCW from previous aerocapture mission studies.

B. Peak Deceleration

During the aerocapture maneuver, the vehicle decelerates rapidly as it descends into the denser region of atmosphere. The peak deceleration load G (in Earth g) to be withstood by the aeroshell structure, orbiter payload, and on board instruments is a critical design parameter for aerocapture missions. The peak deceleration must be less than maximum allowable deceleration $G_{\max}$ set by the mission designer based on the structural and instrument sensitivity considerations.

$$G \leq G_{\max} \tag{3}$$

C. Peak Heat Rate

The aerocapture vehicle needs to withstand aerothermodynamic heating during the atmospheric pass at hypersonic speed. TPS materials protect the orbiter inside the aeroshell from the heating, and the TPS material is chosen based on the peak stagnation-point aerothermal conditions. The convective heating rate $\dot{q}_c$ is estimated using the Sutton–Graves empirical relation [50]:

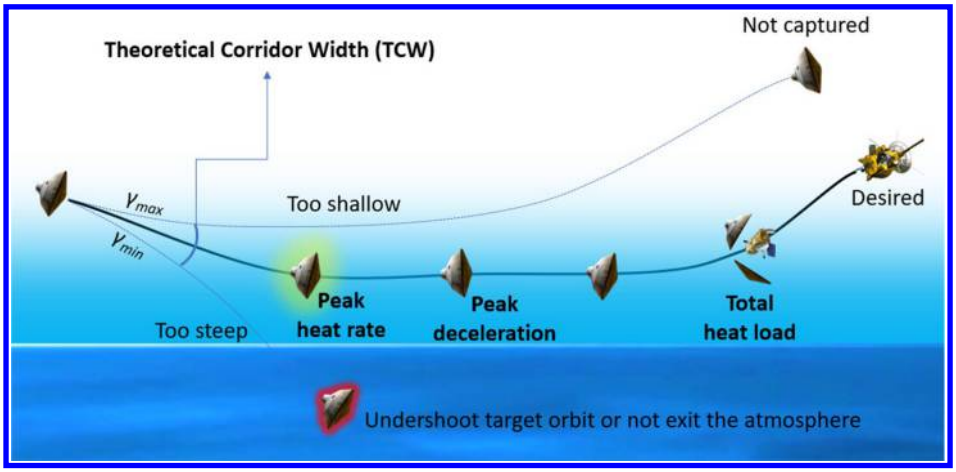

Fig. 2 Theoretical corridor width (TCW) and other aerocapture vehicle design considerations.

Table 1 Nominal delivery errors and TCW from previous studies

Destination	Mission or study	$3-\sigma$ EFPA error, deg	TCW, deg	Reference	Year
Venus	Venus aerocapture (lift)	±0.20	1.52	Lockwood et al. [4]	2006
Venus	Venus aerocapture (drag)	±0.20	0.40	Austin et al. [1]	2019
Earth	Hayabusa	±0.01	— —	Haw et al. [46]	2011
Mars	MSL	±0.01	— —	Martin-Mur et al. [47]	2014
Titan	Titan aerocapture	±0.93	3.50	Way et al. [48]	2003
Neptune	Neptune aerocapture	±0.51	2.00	Starr et al. [49]	2004
Neptune	Neptune aerocapture	±0.33	1.25	Girija et al. [5]	2020

$$\dot{q}_c = K\left(\frac{\rho_\infty}{R_N}\right)^{0.5} V^3 \tag{4}$$

where K is a constant determined by the planet's atmospheric composition, ρ_∞ is the freestream atmospheric density in kilograms per cubic meter, R_N is the vehicle's effective nose radius in meters, and V is the freestream velocity in meters per second. The values of K for the various planets are listed in Table 2. Note that $\dot{q}_c$ has units of watts per square centimeter. The radiative heating rate $\dot{q}_r$ is computed using the correlations from sources listed in Table 2 [51]. Typical values of peak heat rate for lift modulation aerocapture vehicles are in the range of 50–400W/cm^2 at Mars and Titan [21,44], 500–2000W/cm^2 at Venus and Earth [3,52], and 1000–8000W/cm^2 at Uranus and Neptune [5,23]. Reusable TPS materials such as Space Shuttle tiles can withstand about 100 W/cm^2 [53], whereas ablative TPS such as phenolic impregnated carbon ablator (PICA) can accommodate up to about 1200 W/cm^2 [54]. Heatshield for Extreme Entry Environment Technology (HEEET) is a novel 3D woven TPS material and has been tested to about 8000 W/cm^2 under certain laboratory conditions [55].

Drag modulation system uses a low-ballistic coefficient configuration that allows the vehicle to decelerate in the thinner upper regions of the atmosphere and thus keep the heating rates low [28,61]. Drag modulation vehicles can use a jettisonable rigid drag skirt with reusable tiles or PICA or a deployable system such as Adaptable, Deployable, Entry, and Placement Technology (ADEPT) with woven carbon cloth as the TPS. Carbon cloth has been tested to about 250 W/cm^2 [62]. The TPS used for drag modulation vehicles is expected to be able to sustain peak heat rates in the range of 50–1000 W/cm^2. The available TPS material and testing limitations impose the constraint that the peak heat rate is less than the maximum allowable value.

$$\dot{q} \le \dot{q}_{\max} \tag{5}$$

D. Total Heat Load

The stagnation-point heat load Q (the integral of the stagnation-point heat rate for the duration of atmospheric flight) is an important parameter that determines the TPS mass fraction. A higher heat load implies that more TPS thickness is required, hence a higher TPS mass fraction and a lower overall useful payload mass fraction. Using data from flown entry vehicle designs, Laub and Venkatapathy [63] reported a correlation between the stagnation-point heat load Q and TPS mass fraction f_{TPS} for heritage blunt-body aeroshells as follows:

$$f_{\text{TPS}}(\%) = 0.091 Q^{0.51575} \tag{6}$$

in which Q has units of J/cm^2. Equation (6) can be used to approximately estimate the TPS mass fraction, though it is valid only for preliminary conceptual studies. Equation (6) is likely a conservative estimate because state-of-the-art TPS materials such as HEEET are substantially lighter than heritage carbon phenolic (>40%), which was used in a number of missions from which the empirical relation is derived [64]. Higher-fidelity studies can use computational fluid dynamics (CFD) simulations and other thermal analysis packages to refine the TPS distribution and the TPS mass fraction. For initial concept studies, to keep the TPS mass fraction within a reasonable value, the mission designer can specify a maximum allowable heat load:

$$Q \le Q_{\max} \tag{7}$$

Typical values of the total heat load for lift modulation aerocapture range from about 5 to 25 kJ/cm^2 at Mars [21,65]; 10 to 50 kJ/cm^2 at Earth, Venus, and Titan [3]; and 100 to 600 kJ/cm^2 at Uranus and Neptune [5,23]. These heat loads roughly correspond to TPS mass fractions of about 10% at Mars; 10–25% at Earth, Venus, and Titan; and 35–60% at Uranus and Neptune. The validity of the relationship at very high heat loads such as those expected at Uranus and Neptune is not clear, and additional studies are required to determine the TPS mass fraction for aerocapture at these destinations. Venkatapathy et al. [66] performed sizing calculations using PICA and HEEET for a Neptune aerocapture mission using a blunt-body aeroshell and reported TPS mass fraction not exceeding 20% for an arrival V_∞ of 22 km/s. The study also found that conformal PICA is more efficient than HEEET (five times less TPS mass) if the stagnation point peak heat rate is within PICA's tested capability of 1200 W/cm^2. The total heat load attempts to quantify the mass penalty from having to carry a TPS for aerocapture as opposed to conventional propulsive insertion or aerobraking where no TPS is required. This allows a mission designer to compare the delivered mass using different orbit insertion options during the early stages of a mission study when a detailed vehicle design is likely not available.

Table 2 Aerodynamic heating correlations

Planet or moon	Convective heating (value of K) [51]	Radiative heating correlation (source)
Venus	1.8960E-8	Ref. [52]
Earth	1.7623E-8	Ref. [56]
Mars	1.8980E-8	Ref. [52]
Jupiter	0.6556E-8	Ref. [57]
Saturn	0.6356E-8	Ref. [57]
Titan	1.7407E-8	[a]
Uranus	0.6645E-8	Ref. [58]
Neptune	0.6719E-8	Ref. [58]

[a]The radiative heating contribution may be comparable or more than the convective heating at Titan [59,60]. No empirical relations were available and hence not included in the results.

E. Vehicle Design

Aerocapture vehicles require control authority to allow the vehicle to target the desired capture orbit and not risk undershooting or escaping the planet. There are two ways of providing aerodynamic control authority: lift modulation and drag modulation. For the lift modulation technique, the critical vehicle design parameter that dictates control authority is the vehicle lift-to-drag ratio L/D. Most planetary entry vehicles flown to date have L/D in the range of 0–0.40 and are classified as low-L/D vehicles. Low-L/D vehicles have been shown to provide sufficient control authority at Venus, Earth, Mars, and Titan [4,21,22]. Aerocapture studies at Uranus and Neptune have traditionally used mid-L/D vehicles with L/D in the range of 0.6–0.8 [23], though recent work [5,31] has shown that improvements in delivery errors, and guidance schemes can reduce the L/D requirement. Another important vehicle design parameter is the vehicle ballistic coefficient β. A vehicle with a lower ballistic coefficient will slow down higher up in the atmosphere where it is thinner, and encounters lower peak heat rates as compared to a high ballistic coefficient vehicle. Typical values of β for rigid blunt-body aeroshells fall in the range of 150 (MSL)–400 (Apollo) kg/m^2 [65,67]. The present study assumes a nominal value of $\beta =$ 200 kg/m^2 for all the lift modulation results.

For drag modulation, the vehicle control authority is determined by the ballistic coefficient ratio after and before drag skirt separation β_2/β_1. In a simple discrete event drag modulation vehicle, the ballistic coefficient is allowed to take two values: a small value β_1 with the drag skirt on and a high value β_2 after the drag skirt is jettisoned [28]. The present study assumes that the drag modulation technique is used to insert a small satellite (<200 kg) into orbit such as the one studied by Austin et al. [1], and uses a nominal value of $\beta_1 = 20$ kg/m^2 for all the drag modulation cases.

Another important vehicle design parameter is the effective nose radius R_N, which strongly affects the stagnation point heat rate as seen in Eq. (4). The present study assumes that $R_N = 1.0$ m, which is comparable to the MSL geometry for all the lift modulation results, and $R_N = 0.1$ m (based on Ref. [1]) for all the drag modulation cases.

F. Atmosphere Models

The present study uses mean density profiles from the Global Reference Atmospheric Models (GRAMs) for Venus, Earth, Mars, Titan, and Neptune. GRAMs are engineering-level atmosphere models developed by NASA Marshall Spaceflight Center and are widely used for analysis of flight trajectories in planetary atmospheres [68–71]. For Jupiter, data from the Galileo Atmospheric Structure Instrument (ASI) is used [72]. For Saturn, a nominal atmospheric profile from Voyager radio occultation measurements is used [73]. For Uranus, a nominal atmospheric profile developed by NASA Ames Research Center for entry probe studies and made available to the authors is used [74].

For preliminary mission studies, it is sufficient to use a nominal mean density profile for aerocapture trajectory analysis as done in the present work. Higher-fidelity studies to quantify guidance performance will need to include the effect of mean density variations, uncertainty in mean profiles, and high-frequency density perturbations in the atmosphere model [5]. Table 3 lists the models used in the study** and the height of the atmospheric interface at which the TCW values are reported in Sec. IV.

H. Interplanetary Arrival Conditions and Target Capture Orbit

The arrival V_∞ is an important parameter that characterizes the interplanetary trajectory. The arrival V_∞ determines the planet-relative entry speed at the atmospheric entry interface, which in turn determines the available TCW, deceleration, and heating encountered by the aerocapture vehicle. Typical arrival V_∞ values are less than 6 km/s for targets such as Venus and Mars [3], and less than about 12 km/s in the outer solar system for propulsive insertion architectures [5,30]. The present study considers a wide range of arrival V_∞ for every planetary destination. The wide range is chosen to accommodate scenarios such as a small satellite being delivered to Venus by a mother spacecraft that is using Venus as a gravity-assist body on its way to the outer solar system. Another scenario would be a very short time-of-flight (<6 years), high-energy trajectory to Neptune that arrives with a V_∞ of 20 km/s or more. Table 4 lists the target capture orbits for the various destinations considered in the study and are based on previous aerocapture and other mission concept studies.

For outer planet missions such as those to Uranus and Neptune, typical propulsive insertion architectures generally use a highly elliptical (period >100 days) capture orbit to minimize the orbit insertion ΔV and hence the required propellant mass. Such large initial capture orbits are not practical for aerocapture, as the margin between getting captured and escaping is too small at atmospheric exit. For example, aerocapture at Neptune into a 3-day orbit with a target apoapsis altitude of 400,000 km results in $v_{\text{exit}}/v_{\text{escape}}$ of 0.97, which is high but still provides acceptable margin [5,23]. For a 100-day orbit, with a target apoapsis altitude of 4 million km, $v_{\text{exit}}/v_{\text{escape}}$ exceeds 0.99 and presents a substantial risk of the vehicle not getting captured considering large atmospheric uncertainties at Neptune.

III. Interplanetary Trajectory Trade Space

A database of interplanetary trajectories to Venus, Uranus, and Neptune was compiled to assess the range of arrival V_∞ values for each destination and provide a catalog of trajectories for rapid mission studies. The interplanetary trajectory study was limited to these destinations because of the time constraints of this study, and these destinations are representative of an inner planet and an outer planet mission using aerocapture. The interplanetary trajectories from Earth to Venus were generated using the Satellite Tour Design (STOUR) software developed at Jet Propulsion Laboratory and upgraded at Purdue University for automated design of gravity assist trajectories [75]. STOUR is a patched conic tool that allows multiple body gravity assist sequences along with user-specified ΔV constraints and has widely been used in preliminary mission studies [76–78]. Trajectory data for Uranus and Neptune come from two sources: the NASA Ice Giants Pre-Decadal Mission Study [30], and a set of high V_∞ trajectories computed at the Jet Propulsion Laboratory and made available to the authors during the same study. In addition to the arrival V_∞, two other important parameters for an interplanetary trajectory are the launch C_3, which dictates the launch mass capability for a given launch vehicle, and the time of flight, which is of great importance for outer planet missions. Tradeoffs between the launch C_3, time of flight, and arrival V_∞ and their implications for aerocapture mission design are discussed for the various destinations considered.

Table 3 Atmospheric models and entry interface definition

Planet or moon	Atmosphere model	Entry interface (height above surface, km)
Venus	Venus-GRAM	150
Earth	Earth-GRAM	140
Mars	Mars-GRAM	120
Jupiter	Galileo ASI data	1000[a]
Saturn	Voyager radio occultation data	1000[a]
Titan	Titan-GRAM	1000
Uranus	Ames model	1000[a]
Neptune	Neptune-GRAM	1000[a]

[a]Surface defined at the 1 bar pressure level.

Table 4 Target capture orbits

	Target orbit periapsis × apoapsis, km	
Planet or moon	Lift modulation	Drag modulation
Venus	400 × 400	400 × 400
Earth	400 × 400	400 × 400
Mars	400 × 400	400 × 400
Jupiter	4,000 × 430,000	4,000 × 4,000
Saturn	4,000 × 265,000	4,000 × 4,000
Titan	1,700 × 1,700	1,700 × 1,700
Uranus	4,000 × 903,323[a]	4,000 × 4,000[b]
Neptune	4,000 × 400,000[c]	4,000 × 4,000[b]

[a]Based on an assumed 10-day science orbit.
[b]Based on an assumed close-in orbit for a small spacecraft.
[c]Based on an orbit that permits Triton flybys [5,23].

A. Venus

Figure 3 shows the interplanetary trajectory trade space for Earth–Venus transfers. Launch dates spanning a period of 8 years (2018–2026) are chosen, as the Earth–Venus orbital configuration

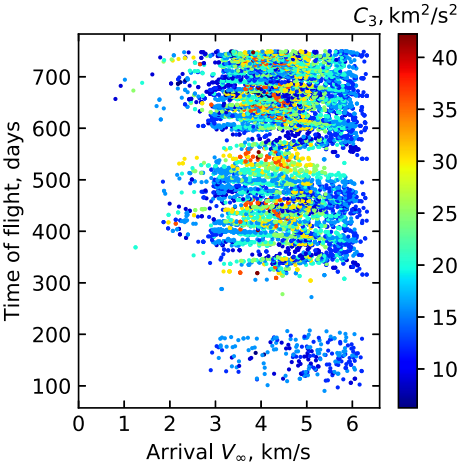

Fig. 3 Trade space for Venus interplanetary trajectories.

**Atmosphere models used in the study are available online at https://github.com/athulpg007/AMAT/tree/master/atmdata.

approximately repeats every 8 Earth years and the results are representative of the wide range of launch and arrival conditions [79].

The results are for ballistic transfers from Earth to Venus, and with up to one deep-space maneuver (DSM) and one Venus flyby. The trajectories with time of flights between 100 and 200 days are the direct Earth–Venus transfers, whereas those in the range of 300–700 days correspond to trajectories with a Venus flyby and a deep space maneuver before arrival at Venus. The range of arrival V_∞ is 2–6 km/s for Earth–Venus trajectories as seen in Fig. 3.

B. Uranus and Neptune

Figures 4 and 5 show the trajectory trade space for Uranus and Neptune, respectively. The trajectories are divided into two classes: 1) a set of low-C_3, low-arrival-V_∞, ballistic, and solar electric propulsion trajectories shown in blue, and 2) a set of high-C_3, high-arrival-V_∞ (12–25 km/s) ballistic trajectories shown in the color range from green to red. The first class is well suited for propulsive insertion architectures as the low arrival V_∞ keeps the orbit insertion ΔV as small as possible and hence the propellant mass low. The first class of trajectories has C_3 in the range of 10–75 km^2/s^2 and is suitable when the largest launch vehicles available are Atlas V551 or similar.

The second class of trajectories becomes feasible only if aerocapture is considered, as propulsive insertion becomes infeasible for arrival V_∞ of 12 km/s or higher as will be shown in Sec. V.E. The second class is characterized by high C_3 in the range of 75–200 km^2/s^2 and requires the use of launch vehicles such as the Delta IV Heavy, Falcon Heavy, or the Space Launch System (SLS). For a launch C_3 of 100 km^2/s^2, the second class of trajectories can enable flight times as low as 6 years to Uranus and as low as 8 years to Neptune. The high arrival V_∞ reduces the vehicle L/D requirement as will be shown in Sec. IV.G, though the high entry speeds also result in substantial aerothermal loads. Preliminary calculations indicate that existing TPS materials such as HEEET can accommodate arrival V_∞ values up to about 23 km/s at Uranus and Neptune.

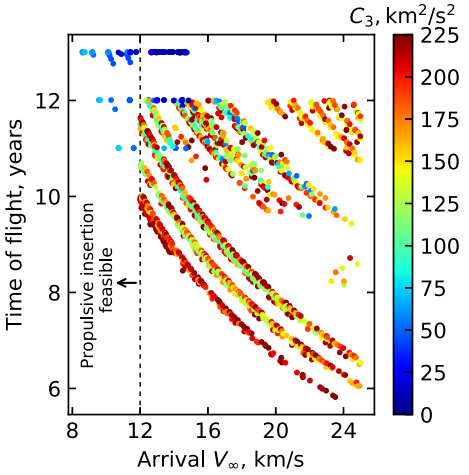

Fig. 4 Trade space for Uranus interplanetary trajectories.

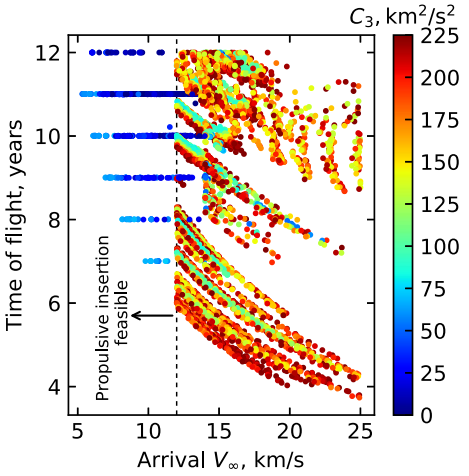

Fig. 5 Trade space for Neptune interplanetary trajectories.

IV. Aerocapture Feasibility Charts

Aerocapture feasibility charts are presented in this section for lift and drag modulation aerocapture at Venus, Earth, Mars, Jupiter, Saturn, Titan, Uranus, and Neptune. The vehicle control authority and heating environments are strongly destination dependent, and these charts enable a quantitative comparison of the feasibility of aerocapture across the solar system. Table 5 summarizes the range of constraint values for TCW and peak deceleration considered in this section. Additional charts with more contour levels are presented in the Appendix.

A. Venus

Figure 6a shows the lift modulation aerocapture feasibility chart for Venus with a selected set of constraint values. The green-shaded region indicates the feasible set of L/D and arrival V_∞ for TCW requirement of 1.0 deg. If the TCW requirement can be reduced to 0.5 deg by improvements in approach navigation, for example, the vehicle control requirements can be relaxed and aerocapture can be accomplished with a lower L/D vehicle as indicated by the yellow region. Typical values of arrival V_∞ fall in the range of 2–6 km/s for Earth–Venus transfers [3], though gravity assist flybys of Venus could have much higher V_∞. Figure 6a shows that heritage blunt-body aeroshells with L/D in the range 0.1–0.4 offer sufficient control authority for aerocapture at Venus, which implies that heritage aeroshell designs such as Viking, Apollo, MSL, and Orion can be leveraged for future Venus missions [65,67,80,81]. Figure 6a allows the mission designer to quantitatively estimate the required vehicle L/D based on the required TCW and arrival V_∞, while staying within the deceleration and heating constraints. The peak heat rates at Venus are higher compared to Earth because of the different atmospheric characteristics, but are within the capability of PICA for V_∞ of up to about 5 km/s, and within the capability of HEEET for V_∞ of up to about 10 km/s. For the shaded region, the stagnation-point total heat load does not exceed 50 kJ/cm^2, which implies that expected TPS mass fraction is less than 24% based on Eq. (6).

Figure 6b shows the drag modulation feasibility chart for Venus. The TCW for drag modulation technique ($\beta_2/\beta_1 < 10$) is generally smaller than that for lift modulation vehicles ($L/D < 0.4$). If the TCW requirement is 0.60 deg, the required vehicle β_2/β_1 is about 20. If the TCW requirement is lowered to 0.30 deg, a vehicle with β_2/β_1 of approximately four can provide the required control authority. For comparison, the Venus drag modulation concept studied by Austin et al. [1] used a β_2/β_1 of 9.2 to accommodate a ± 0.2 deg EFPA uncertainty at the entry interface. The selected peak heat rate

Table 5 TCW values used in the feasibility charts

Planet or moon	TCW, deg		Peak heat rate, W/cm^2	
	Lift modulation[a]	Drag modulation[b]	Lift modulation	Drag modulation
Venus	0.5–1.0	0.3–0.6	1,000–5,000	400–600
Earth	0.5–1.0	0.3–0.6	1,000–5,000	400–600
Mars	0.5–1.0	0.3–0.6	300–800	200–600
Jupiter	0.2–0.5	0.3–0.4	12,000–16,000	9,000–10,000
Saturn	0.5–1.0	1.0–1.5	1,600–3,200	1,800–2,100
Titan	0.5–1.0	1.0–2.0	100–400	70–200
Uranus	1.0–2.0	0.5–1.0	2,000–7,000	1,200–1,600
Neptune	1.0–2.0	0.5–1.0	2,000–7,000	1,200–1,600

[a]TCW range based on the discussion in Sec. II.A.

[b]Based on the available TCW for the range of β_2/β_1 and V_∞ considered.

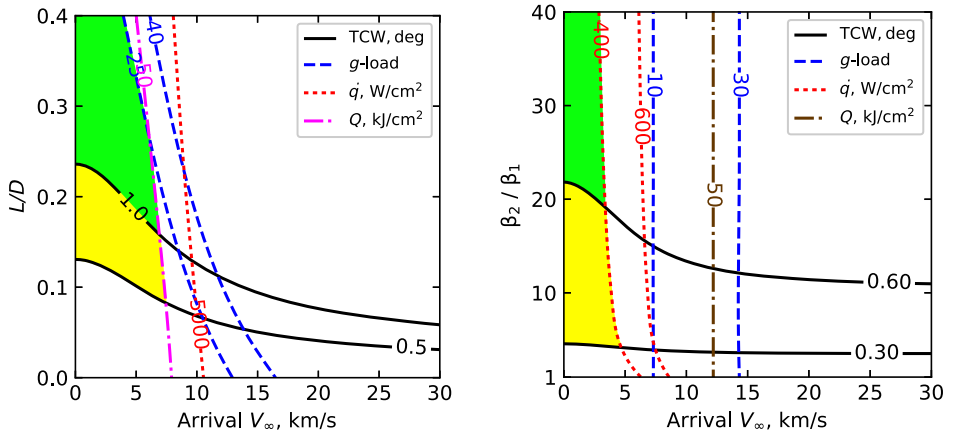

a) Lift modulation b) Drag modulation

Fig. 6 Aerocapture feasibility charts for Venus. The green region in the left figure indicates the feasible $(L/D, V_\infty)$ for lift modulation aerocapture with a TCW requirement of 1 deg. With a required TCW of 0.50 deg, the yellow region also becomes feasible.

constraint of 400 W/cm^2 (a nominal upper limit for carbon-cloth TPS used in deployable drag modulation system derived from ADEPT) limits the arrival V_∞ to about 5 km/s. If a rigid drag skirt with PICA TPS is used, it is possible to accommodate V_∞ of up to about 10 km/s. Drag modulation is an attractive option to insert small rideshare satellites into Venus orbit from a larger mission that uses Venus for gravity assist [1,82].

B. Earth

Figure 7a shows the lift modulation chart for Earth and is similar to Venus (Fig. 6a) except for the less-demanding heating environment. The shaded feasible region indicates that heritage low-L/D vehicles (L/D of 0.1–0.4) offer sufficient control authority at Earth for the aerocapture maneuver. For the selected heat rate constraint of 1000 W/cm^2, which can be accommodated by PICA, the arrival V_∞ is limited to about 8 km/s. For a potential sample return mission from the outer solar system that has a higher V_∞ of about 12 km/s and peak heat rate of about 5000 W/cm^2, HEEET TPS can be used. Aerocapture at Earth is of particular interest for two mission categories: an aerocapture demonstration at Earth as proposed by Hall [18] and Keys [19], and a sample return from a solar system target that is desired to be captured into Earth orbit instead of bringing the samples to the surface for planetary protection reasons.

Figure 7b shows the drag modulation chart for Earth. Earth's well-known atmosphere and small EFPA uncertainties compared to planetary destinations make the vehicle control authority requirements the least demanding. As seen from the shaded region in Fig. 7b, ballistic coefficient β_2/β_1 ratios as small as five offer sufficient control authority if the TCW requirement is 0.6 deg. For TCW requirement of 0.3 deg the β_2/β_1 ratio can be reduced to two. The peak heat rates are well within the capability of PICA for V_∞ less than 10 km/s, and for smaller values of V_∞, carbon cloth may be sufficient, enabling a deployable system such as ADEPT to be used. Drag modulation at Earth is particularly attractive as an option to demonstrate a low-cost end-to-end aerocapture mission using a SmallSat. Werner and Braun [36] studied such a SmallSat mission concept with a β_2/β_1 ratio of 4.5 and a jettisionable drag skirt with PICA TPS. The SmallSat would fly as a secondary payload on a Geosynchronous Transfer Orbit (GTO) launch and then demonstrate aerocapture, thus greatly reducing the cost of such a mission.

C. Mars

Figure 8a shows the lift modulation chart for Mars, and it is similar to that for Venus and Earth, but with significantly less demanding aerothermal loads. Low L/D vehicles once again offer sufficient control authority as seen from the shaded feasible regions, and the peak heat rates are well within the capability of PICA. The MSL aeroshell design ($L/D = 0.24$, PICA TPS) may be readily adapted to a future Mars aerocapture vehicle. Spilker et al. [7] point out that the hypersonic maneuvering capabilities for precision landing demonstrated by MSL at Mars are more challenging than that required for aerocapture. The relatively benign peak heat rates and experience with entry systems make Mars another attractive destination for future technology demonstration missions after Earth. Fujita and Narita [27] have studied a small-sized Mars aerocapture demonstrator concept with $L/D = 0.2$ and a nonablative lightweight TPS that

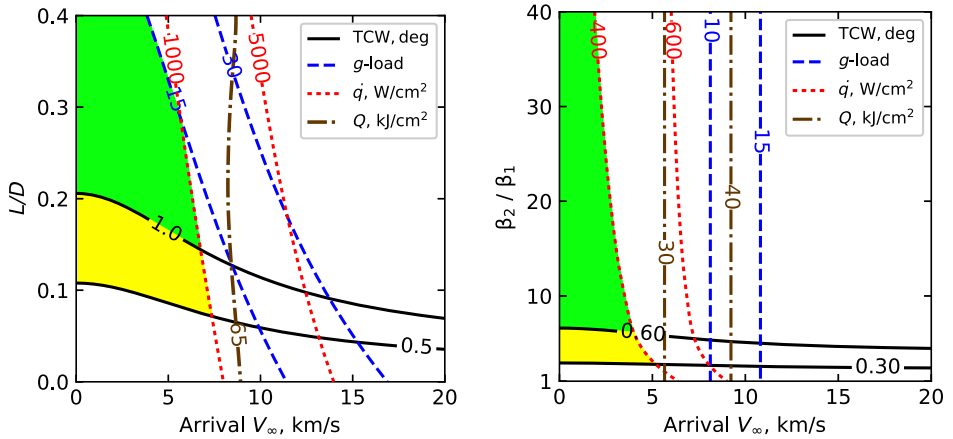

a) Lift modulation b) Drag modulation

Fig. 7 Aerocapture feasibility charts for Earth.

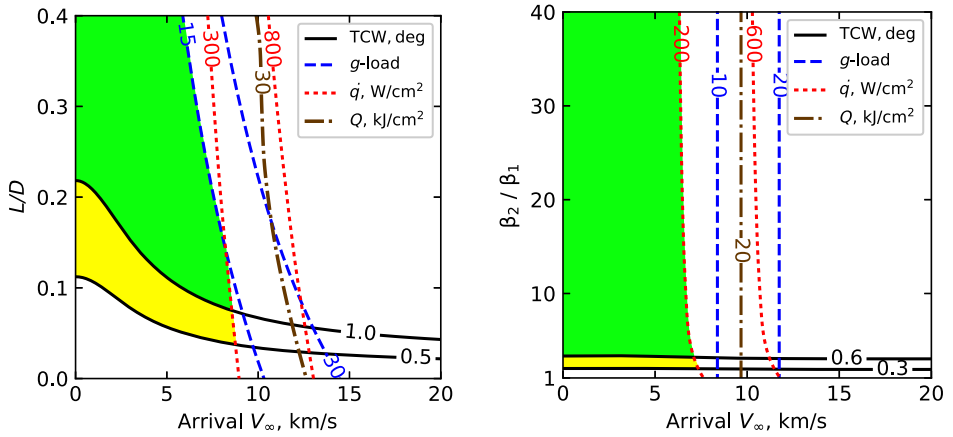

a) Lift modulation b) Drag modulation

Fig. 8 Aerocapture feasibility charts for Mars.

could sustain the expected peak heat rate of 50 W/cm^2. Future, more ambitious missions using aerocapture at Mars may be able to deliver a lander or rover and an orbiter using a single aeroshell similar to the concept studied by Hassett [83] in the 1980s. The propellant savings offered by aerocapture compared for such large and complex missions such as SR, and future manned missions make it an attractive option to be considered in future mission studies [24,84].

Figure 8b shows the drag modulation chart for Mars, which is similar to that for Earth (Fig. 7b), but with a much more benign heating environment. The shaded region indicates that ballistic coefficient ratios as small as three may be sufficient to provide the required control authority at Mars while keeping the peak heat rate below 200 W/cm^2. Putnam and Braun [28] has extensively analyzed drag modulation flight performance for Mars missions. Werner and Braun [36] analyzed the performance drag modulation system with $\beta_2/\beta_1 = 4.5$ designed for Earth demonstration, and found comparable performance for the system at Mars. With its relatively benign heating environment and excellent control authority provided by low β_2/β_1 vehicles, Mars presents an attractive opportunity for a low-cost aerocapture demonstration at a planetary target. Falcone et al. [2] analyzed a low-cost SmallSat mission concept using drag modulation at Mars with a β_2/β_1 ratio of 9, and reported peak heat rates less than 100 W/cm^2.

D. Jupiter

Figure 9a shows the lift modulation aerocapture feasibility chart for Jupiter. Jupiter's large gravity well results in planet-relative entry speeds in excess of 50 km/s and presents extremely high heat rates and heat loads on the entry vehicle. The harsh aerothermal environment for aerocapture at Jupiter makes it challenging to perform aerocapture, and propulsive insertion is the preferred orbit insertion method for the foreseeable future. The available corridor width is much smaller compared to that of Earth or Mars, and low-L/D blunt-body aeroshells do not offer sufficient control authority at Jupiter. For these reasons, aerocapture is considered by experts as long-term goal when there are significant advances in TPS materials capable of handling such extreme entry conditions [7].

Figure 9b shows the drag modulation chart for Jupiter. Once again, the extremely high peak heat rate exceeding 10,000 W/cm^2 is considered beyond the capability of any existing TPS materials used on drag modulation systems. The available corridor width is also quite small. A ballistic coefficient ratio of 20 is required even for a very low TCW of 0.4 deg. These factors make drag modulation aerocapture at Jupiter infeasible in the near-term, and it is not of practical interest for missions to Jupiter for the foreseeable future.

E. Saturn

Figure 10a shows the lift modulation aerocapture feasibility chart for Saturn, which is quite similar to that of Jupiter (Fig. 9a), but with less severe aerothermal conditions. For a TCW requirement of 1 deg, mid-L/D vehicles are required to provide sufficient control authority except at high arrival V_∞ (>15 km/s) where blunt-body aeroshells might be sufficient. The peak heat rate is within the capability of HEEET. Although aerocapture at Saturn appears feasible, it is well known that performing aerocapture or aerogravity assist at Titan is a much more attractive option [85].

Figure 10b shows the drag modulation chart for Saturn. The peak heat rates are not as high as that at Jupiter, but still are quite

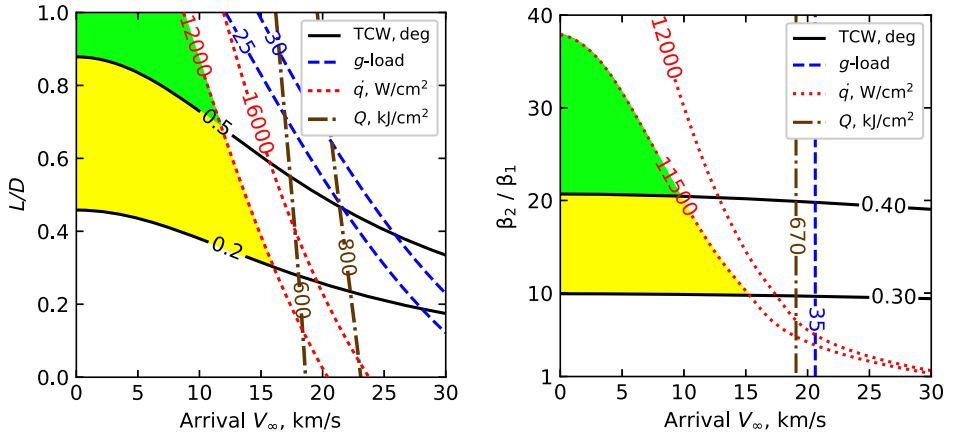

a) Lift modulation b) Drag modulation

Fig. 9 Aerocapture feasibility charts for Jupiter.

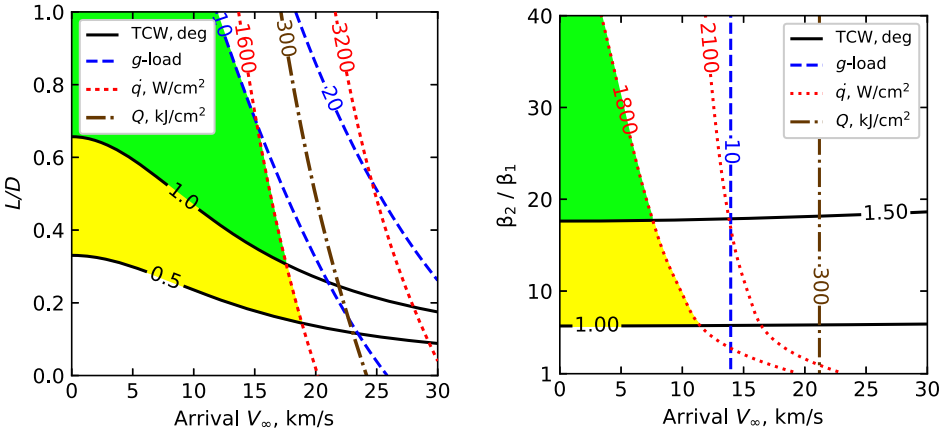

a) Lift modulation b) Drag modulation

Fig. 10 Aerocapture feasibility charts for Saturn.

high values for drag modulation systems, making them an infeasible option for aerocapture at Saturn. As explained in Sec. IV.F, it is desirable to use Titan's atmosphere to achieve orbit insertion at Saturn.

F. Titan

Figure 11a shows the lift modulation aerocapture feasibility chart for Titan, and it is similar to that for Mars (Fig. 8a). Titan's low gravity and the extended dense atmosphere result in large-scale heights, which enable vehicles with L/D as small as 0.1 to provide excellent control authority. The low gravity also implies that the planet-relative entry speeds are low, resulting in benign heating rates even less than that for Mars. The large available TCW and very low peak heat rates make Titan the least demanding destination for aerocapture in our solar system [7]. Lu and Saikia [44] have extensively studied the feasibility of lift modulation aerocapture for future Titan missions. Spilker et al. [7] concluded that aerocapture at Titan can be accomplished using existing aeroshells and TPS, and no new technology development efforts would be required other than engineering developments common to any mission.

Figure 11b shows the drag modulation chart for Titan, which is similar to that for Mars (Fig. 8b). For a TCW requirement of 0.6 deg, vehicles with β_2/β_1 as low as two provide sufficient control authority. The heat rates are even lower than that for Mars, making Titan an attractive destination for drag modulation aerocapture. Putnam and Braun [28] have extensively analyzed the aerothermal environment and flight performance for drag modulation aerocapture vehicles at Titan. Future missions may use drag modulation aerocapture to insert multiple small satellites into appropriate Titan orbits such as those for low-altitude global mapping constellations or communication relays for surface missions [2].

G. Uranus

Figure 12a shows the lift modulation aerocapture feasibility chart for Uranus. The green-shaded region indicates that, for TCW requirement of 2 deg, vehicles with L/D in the range of 0.6–0.8 are required to provide sufficient control authority. Such mid-L/D vehicles have not yet been flown on planetary missions and will require significant development and testing. The lack of a flown mid-L/D vehicle presents a major hurdle for aerocapture at Uranus (and Neptune). Heritage blunt-body aeroshells such as Apollo entry vehicle have L/D values less than 0.40. If the TCW requirement is lowered to 1 deg, the yellow region becomes feasible lowering the L/D requirement, and vehicles with $L/D = 0.40$ offer sufficient control authority for high values of arrival V_∞. It is worth noting that interplanetary trajectories with V_∞ less than a critical value (defined for a given TCW requirement and L/D) are infeasible for aerocapture missions due to lack of control authority. For example, for TCW = 1 deg and $L/D = 0.4$, the minimum required arrival V_∞ is about 17 km/s as seen in Fig. 12a. For a trajectory with arrival V_∞ of about 10 km/s (which is typical for architectures with propulsive insertion [30]), aerocapture is infeasible even with a mid-L/D vehicle.

The expected peak heat rates are in the range of a few to several thousand watts per square centimeter, and HEEET is the only candidate TPS material. PICA may be sufficient in certain situations with less demanding entry conditions such as at the low end of feasible arrival V_∞, and near-equatorial prograde entry. Selecting a high arrival V_∞ to lower the vehicle L/D requirement must be carefully

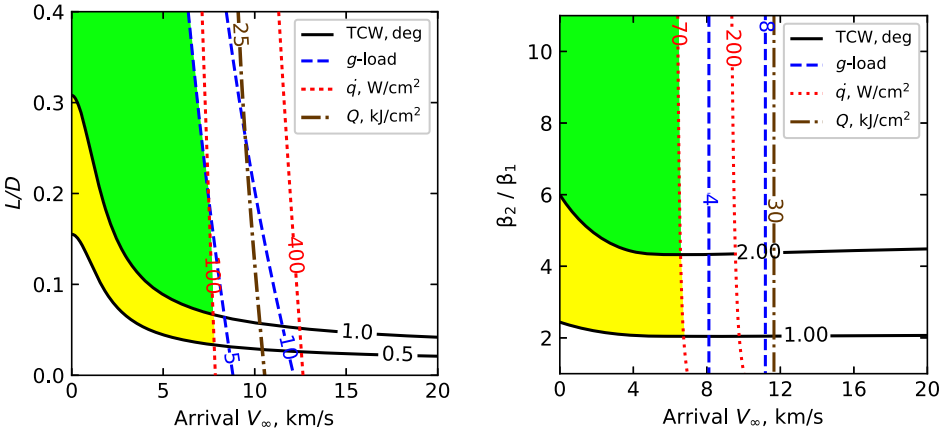

a) Lift modulation b) Drag modulation

Fig. 11 Aerocapture feasibility charts for Titan.

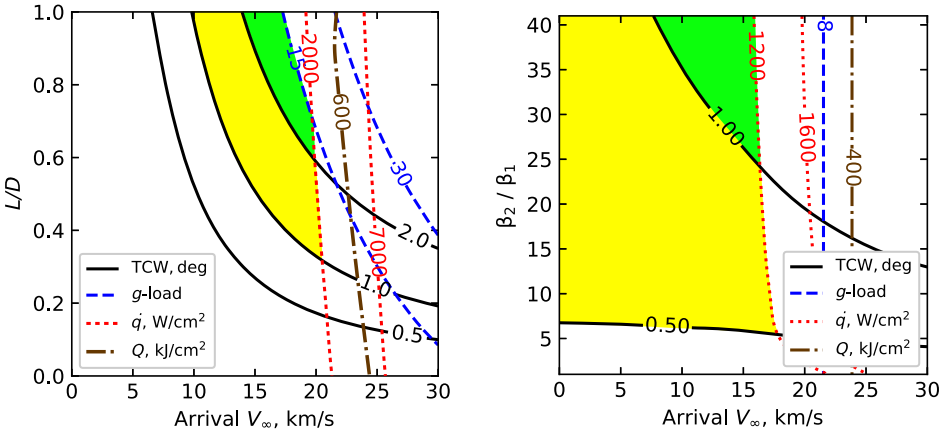

a) Lift modulation b) Drag modulation

Fig. 12 Aerocapture feasibility charts for Uranus.

balanced against the proximity to the peak heat-rate constraint boundaries. Figure 12a neglects the effects of planetary rotation for simplicity, but the entry latitude and orientation are known to affect heat rates substantially for Uranus and Neptune when planetary rotation is included [5]. Higher-fidelity studies must account for these effects when selecting TPS materials for aerocapture at the ice giants.

Figure 12b shows the drag modulation chart for Uranus. A ballistic coefficient ratio of 25 is required to achieve 1.0 deg TCW at an arrival V_∞ of 15 km/s. Lowering the TCW requirement to 0.5 deg would allow ballistic coefficient ratio of about 7 to be feasible. The peak heat constraint of 1200 W/cm^2 limits the maximum arrival V_∞ to about 17 km/s. Given the large atmospheric uncertainties to be expected at Uranus, the delivery EFPA errors would likely have to be driven down to an order of magnitude lower than what is possible with existing navigation technologies [5]. Autonomous navigation (AutoNAV) technology that removes the requirement for ground in the loop in tracking and trajectory correction maneuvers (TCMs) may allow such tight tolerances on EFPA to be achieved [86]. Similar studies addressing the EFPA errors have been performed for drag modulation aerocapture at Venus [1], and extension of these results to Uranus and Neptune is recommended for future studies.

H. Neptune

Figure 13a shows the lift modulation feasibility chart for Neptune, and it is similar to that for Uranus (Fig. 12a). The green-shaded region indicated that vehicle L/D in the range of 0.6–0.8 is required for TCW requirement of 2 deg as concluded by Lockwood et al. [23] in 2006. For TCW requirement of 1 deg, the feasible region expands to include the yellow-shaded area. Recent work has indicated that using a trajectory with arrival V_∞ of 20 km/s coupled with improvements in navigation and guidance can reduce the L/D requirement to 0.3–0.4, enabling heritage blunt-body aeroshells such as Apollo to perform aerocapture at Neptune [5]. The expected peak heat rates for Neptune aerocapture fall in the range of 1000–8000 W/cm^2, which requires the use of HEEET TPS, or PICA in some conditions at the lower end of the range. Neptune's large gravity well results in planet-relative entry speeds in the range of 27–33 km/s and heat loads in the range of few to several hundred kilojoules per square centimeter. Additional study is required to ascertain if the TPS mass fraction can be kept within an acceptable level for such large total heat loads.

Aerocapture was considered a potentially enhancing new technology by the Ice Giants Pre-Decadal Mission Study, which investigated both Uranus and Neptune mission concepts [30]. Missions to Uranus and Neptune stand to benefit the most from aerocapture owing to their large heliocentric distances. In addition to delivering substantially more mass than propulsive architectures, aerocapture can enable a new class of short-time-of-flight, fast-arrival-V_∞ trajectories that are infeasible with propulsive insertion. When combined with aerocapture, the SLS would enable trip times to Uranus and Neptune to be as short as 5 and 7 years, respectively [87].

Figure 13b shows the drag modulation chart for Neptune. Vehicles with β_2/β_1 of 15 or more provide sufficient control authority for TCW requirement of 1.0 deg or less. Additional study is required to ascertain if a small satellite using drag modulation can achieve the tight EFPA error requirements required to meet this TCW requirement. As is the case with Uranus, deployment of small satellites into

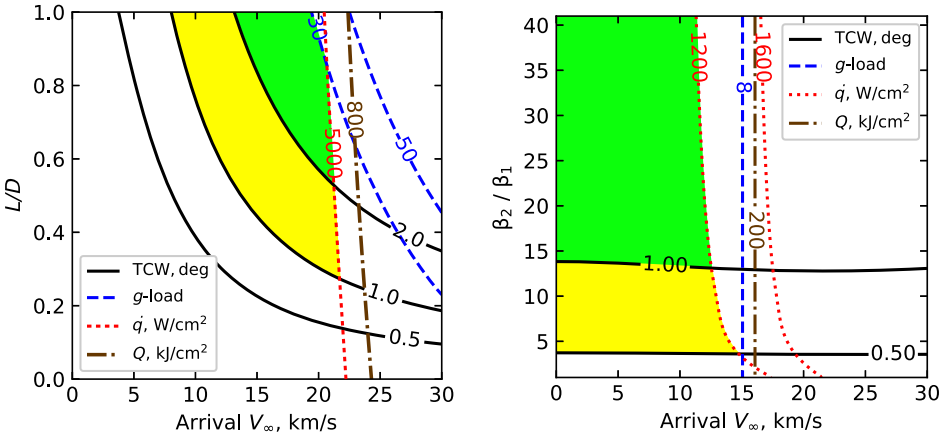

a) Lift modulation b) Drag modulation

Fig. 13 Aerocapture feasibility charts for Neptune.

different orbits from a mother spacecraft on arrival or after orbit insertion using drag modulation may be possible and is worth future investigation. The considered peak heat rate constraint of 1200 W/cm^2 though a high value for drag modulation systems can only accommodate arrival V_∞ up to about 13 km/s.

V. Mass-Benefit Analysis

The mass benefit offered by aerocapture depends on the destination and the interplanetary arrival V_∞. Though aerocapture offers savings in terms of propellant mass, the aeroshell structure that encloses the payload and the heat shield impose a mass penalty and must be considered in mission concept studies. This section compares the delivered mass to orbit for the atmosphere-bearing destinations using three orbit insertion techniques: 1) purely propulsive orbit insertion to the target orbit, 2) propulsive insertion to a large elliptical orbit followed by aerobraking to the target orbit, and 3) aerocapture into the target orbit. For purely propulsive insertion and propulsive insertion followed by aerobraking, the useful payload mass fraction $f_{P,\text{prop}}$ defined as the fraction of arrival mass (before orbit insertion) that is inserted into orbit is [3]

$$f_{P,\text{prop}} = 1 - 1.12\left(1 - \exp\left[-\frac{\Delta V_{\text{OI}}}{I_{\text{sp}} g_0}\right]\right) \tag{8}$$

where 1.12 is an assumed tankage factor to account for the structural mass of the propulsion system, ΔV_{OI} is the orbit insertion ΔV, I_{sp} is the propulsion system specific impulse, and $g_0 = 9.80665$ m/s^2 is the standard free-fall acceleration. The orbit insertion ΔV is computed as

$$\Delta V_{\text{OI}} = \sqrt{V_\infty^2 + \frac{2\mu_p}{r_{\text{pe}}}} - V_{\text{pe}} \tag{9}$$

where μ_p is the standard gravitational parameter, r_{pe} is the periapsis radius of the target capture orbit, and V_{pe} is the orbital speed at periapsis of the target capture orbit. The study uses an $I_{\text{sp}} = 320$ s assuming a conventional bipropellant engine. For purely propulsive insertion, V_{pe} is the periapsis speed of the target capture orbits defined in Table 4 under the lift modulation heading. For aerobraking, V_{pe} is the periapsis speed of an intermediate capture orbit defined in Table 6. The spacecraft will, over the course of several weeks or months, make multiple aerobraking passes in the upper atmosphere during each periapsis pass to gradually reduce the apoapsis to that of the target capture orbits defined in Table 4. For aerobraking, the entire mass delivered to the initial large orbit is assumed delivered to the smaller target orbit after the aerobraking period.

In addition to TPS materials, the entry vehicle for aerocapture includes aeroshell structure, guidance and navigation systems, and other supporting equipment that is not considered useful payload delivered to orbit. All such systems (excluding the TPS materials) essential for entry vehicle function but not usable payload are lumped into a single parameter called entry support system mass M_{ESS}. The total aerocapture vehicle entry mass is

Table 6 Initial capture orbits for aerobraking

Planet or moon	Periapsis × apoapsis altitude, km
Venus	400 × 60,000
Earth	400 × 60,000
Mars	400 × 60,000
Titan	1,700 × 300,000
Uranus	4,000 × 4,962,409[a]
Neptune	4,000 × 5,248,815

[a]Based on an assumed 120-day initial orbit.

$$M_{\text{Total}} = M_{\text{ESS}} + M_{\text{TPS}} + M_P \tag{10}$$

where M_{TPS} is the TPS mass, and M_P is the useful payload mass. The usable payload mass fraction for the aerocapture vehicle $f_{P,\text{ac}}$ defined as the fraction of arrival mass (before aerocapture) that is delivered to orbit is [3]

$$f_{P,\text{ac}} = 1 - f_{\text{ESS}} - f_{\text{TPS}} \tag{11}$$

where $f_{P,\text{ac}} = M_P/M_{\text{Total}}$, entry support systems mass fraction $f_{\text{ESS}} = M_{\text{ESS}}/M_{\text{Total}}$, and TPS mass fraction $f_{\text{TPS}} = M_{\text{TPS}}/M_{\text{Total}}$. The aerocapture payload mass fraction reported in this study assumes an MSL-derived aeroshell with $f_{\text{ESS}} = 0.23$ [3], and it is only applicable to lift modulation.[††] Drag modulation is not considered in the mass-benefit analysis in this study. The TPS mass fraction is computed using Eq. (6), based on the heat load. For very high heat loads in the range of $200 - 400$ kJ/cm^2 expected at Uranus and Neptune, the TPS mass fraction of 0.50–0.80 from Eq. (6) is likely an overestimate because more recent studies using HEEET have shown that the TPS mass fractions in the range of 0.05–0.20 are feasible for aerocapture at Neptune even with substantially higher heat loads than that for the inner planets [66].

It is noted that there are some limitations to the mass-benefit analysis presented in this section. First, the TPS mass fraction is estimated using a simple empirical relationship derived from historical data. Although this is likely a good estimate for Venus, Mars, and Titan, its applicability to high-heat-load trajectories at Uranus and Neptune may be limited. Second, different TPS materials such as PICA and HEEET can result in significant differences in TPS mass that are not accounted for in this analysis. PICA, for example, is much more mass efficient than HEEET [66]. Third, mass of auxiliary systems such as deployable antennae, aeroshell jettison mechanisms, and propellant mass for post-aerocapture propulsive burns is not considered. Although this study uses a constant entry support system mass fraction, there may be additional structural mass required to sustain the deceleration loads. Even if the aerocapture payload mass fraction is lowered by 0.1 to accommodate a heavier structural mass, the general conclusions still hold for the outer planets.

A. Venus

Figure 14a shows the comparison of payload mass fractions to a 400 × 400 km Venus orbit using the various orbit insertion techniques. For V_∞ in the range of 2–6 km/s, aerobraking delivers the most mass and is the preferred orbit insertion technique. Purely propulsive insertion to a 400 km circular orbit is prohibitive as seen from the very low payload mass fractions. The harsh thermal environment for Venus entry and the large heat loads penalize the aerocapture mass fraction, while aerobraking keeps the orbit insertion ΔV the required propellant mass low. Aerobraking has been demonstrated at Venus by the Magellan and Venus Express missions, and it is planned for the proposed ESA EnVision orbiter and the Venus orbiter mission proposed by the Indian Space Research Organization [88,89]. Aerobraking is the most mass-efficient orbit insertion method at Venus for large missions in the near future. For small short-lived missions (less than a year) whose science requirements demand a low-circular orbit, aerobraking may be infeasible because of the associated time penalty to reach the circular orbit. In this case, aerocapture offers a 100–200% increase in delivered mass compared to purely propulsive insertion (for V_∞ in the range of 2–6 km/s) as seen in Fig. 14a.

Another scenario of interest is the possibility of delivering small satellites to Venus orbit from a spacecraft that uses Venus as a gravity assist body on its way elsewhere in the solar system. Typically such flyby trajectories have much higher V_∞ compared to direct Earth–Venus transfers. Aerocapture outperforms aerobraking for V_∞ in the

[††]The payload mass fraction in this study refers to the useful spacecraft mass (instruments, power, structure, etc.) excluding the propulsion or aerocapture system mass. This is not to be confused with the science payload that only includes the mass of the scientific instruments.

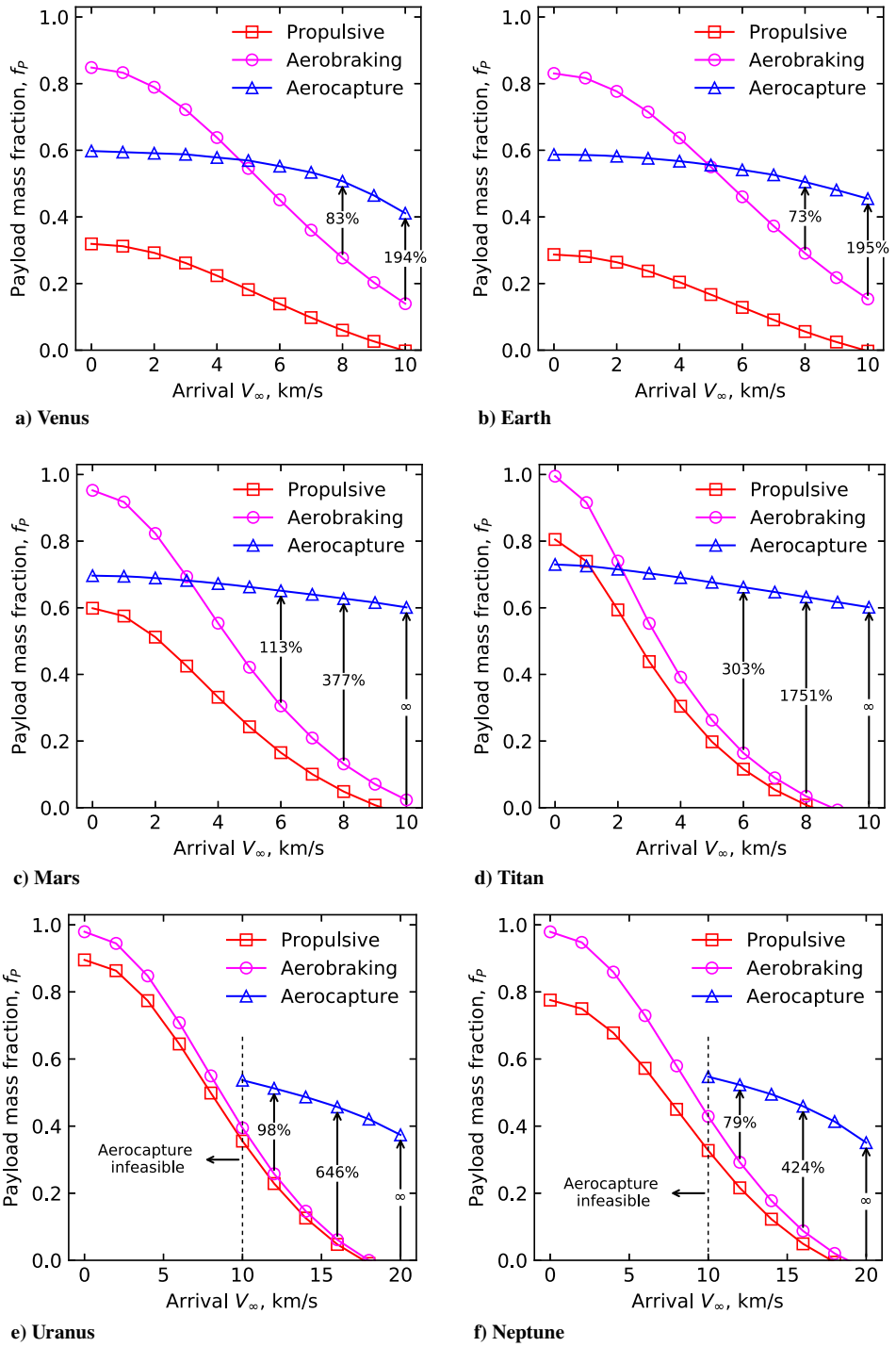

Fig. 14 Payload mass fraction using various orbit insertion techniques.

range of 6–10 km/s, which is typical for spacecraft using Venus as a gravity assist flyby body, and may be used to insert a secondary payload into Venus orbit. For a flyby V_∞ of 8 km/s, aerocapture delivers 83% more mass, and for V_∞ of 10 km/s, 194% more mass compared to aerobraking. For missions that flyby Venus with V_∞ greater than 10 km/s, the peak heat rates exceed that of existing TPS materials and aerocapture is likely infeasible as seen in Fig. 6a.

B. Earth

Figure 14b shows the performance of the different techniques for orbit insertion at Earth, and it is very similar to that for Venus (Fig. 14a). Aerobraking outperforms aerocapture for arrival V_∞ in the range of 0–5 km/s, which is the expected range for return trajectories from the Moon and Mars. However, the repeated passage of the spacecraft through the Van Allen radiation belts is a concern during aerobraking and may place additional demands on the spacecraft in terms of shielding [25]. For crewed missions, both the time penalty and the radiation dose make aerobraking infeasible, and aerocapture is the preferred orbit insertion technique. In the range of V_∞ from 0 to 5 km/s, aerocapture delivers 100–200% more mass to a 400 km circular orbit compared to purely propulsive insertion. For sample return missions from the asteroid belt or elsewhere in the solar system with much higher arrival V_∞, aerocapture clearly outperforms aerobraking. For a mission with arrival V_∞ of 8 km/s, aerocapture delivers 73% more mass, and for an arrival V_∞ of 10 km/s, 195% more mass to a 400 km circular orbit compared to aerobraking.

C. Mars

Figure 14c compares the delivered mass using the different techniques for Mars missions. For low arrival V_∞ in the range of 0–4 km/s, aerobraking is the preferred orbit insertion technique if the time penalty is acceptable. As is the case with Venus, aerocapture can enable orbit insertion into a very-low circular orbit immediately upon arrival, which may be desirable for small satellite missions or CubeSat constellations. The significant heritage associated with aerobraking makes it the preferred orbit insertion technique at Mars for large missions in the near future. For missions with arrival V_∞ in the range of 6–10 km/s, aerocapture outperforms aerobraking. Aerocapture delivers 113% more mass to a 400 km circular orbit compared to aerobraking for V_∞ of 6 km/s. Such high arrival V_∞ trajectories may be of interest to crewed missions that seek to reduce the Earth–Mars transfer time to a few months, or crewed missions that use cycler trajectories. For trajectories with arrival V_∞ of 7 km/s or more, aerocapture is an enabling option as both aerobraking and purely propulsive insertion deliver little useful payload at such high arrival speeds.

D. Titan

Figure 14d compares the delivered mass using the different techniques to 1700×1700 km Titan orbit. For V_∞ in the range of 0–2 km/s aerobraking outperforms aerocapture, but this is not of practical interest as such low arrival speeds at Titan result in very large flight times. When interplanetary trajectories with reasonable flight times are considered, the arrival V_∞ falls in the range of 5–10 km/s. Aerocapture outperforms aerobraking for all speeds in this range, and it is the preferred orbit insertion method both due to the significant mass benefit and the particularly less demanding requirements on the vehicle as mentioned in Sec. IV.F. For V_∞ of 6 km/s, aerocapture delivers 300% more mass compared to aerobraking, and for V_∞ of 8 km/s the percentage increase is nearly 1700%. For trajectories with arrival V_∞ of 10 km/s or more, aerocapture can enable short-time-of-flight Titan missions.

The flexibility in the range of arrival V_∞ offered by aerocapture opens up entirely new class of missions to Titan with flight times as short as three years [22]. Titan's benign aerothermal environment keeps the TPS mass fraction low and delivers substantially more payload to orbit compared to aerobraking or propulsive insertion. The increased payload mass capacity could be leveraged to accommodate multiple elements, such as orbiter, a lander, and one or more aerial platforms, in a single launch vehicle, thus enabling an entirely new class of missions for future Titan exploration.

E. Uranus

Figure 14e compares the delivered mass using the different techniques to a 10-day Uranus orbit. For arrival V_∞ up to about 10 km/s, propulsive insertion can deliver a reasonable payload fraction ($\simeq 0.4$). For arrival V_∞ below 10 km/s, aerocapture is infeasible due to insufficient TCW as shown in Fig. 12a. Note that the above conclusion is valid only for lift modulation, and it does not apply to drag modulation aerocapture. For trajectories with arrival V_∞ greater than 10 km/s, aerocapture clearly outperforms aerobraking because the aerobraking delivered mass fraction falls off sharply with increasing V_∞. For an arrival V_∞ of 12 km/s, aerocapture delivers nearly 100% more mass compared to aerobraking. A caveat in this conclusion for V_∞ of 12 km/s is that as seen in Fig. 12a, the required L/D is in the range of 0.6–1.0, for which the structural and TPS mass fractions used in the study do not apply to. For V_∞ of 16 km/s, aerocapture delivers 646% more mass compared to propulsive insertion and may be considered a strongly enhancing to enabling technology. For V_∞ of 20 km/s or higher, propulsive insertion is infeasible, and aerocapture is an enabling technology for orbit insertion from such fast arrival trajectories for missions to Uranus.

As is the case with Titan, aerocapture opens up a class of fast arrival V_∞ interplanetary trajectories for Uranus missions with flight times as low as five years. Trajectories with V_∞ of 20 km/s may enable an Apollo-derived aeroshell with $L/D = 0.40$ to be used for aerocapture at Uranus, and V_∞ of 25 km/s may enable MSL-derived aeroshells with $L/D = 0.24$ to be used as seen from Fig. 12a. The mass savings offered by aerocapture can enable a more capable spacecraft to be inserted into orbit within a substantially shorter flight time than possible with propulsive insertion architectures, along with additional elements such as entry probes and small satellites for a future Uranus mission.

F. Neptune

Figure 14f compares the delivered mass using the different techniques to a $4000 \times 400{,}000$ km Neptune orbit, and it is similar to that for Uranus (Fig. 14e). Propulsive insertion architectures can allow trajectories with arrival V_∞ up to about 10 km/s, beyond which the payload mass fraction falls below 0.40. Aerocapture is infeasible for trajectories with V_∞ up to about 10 km/s due to lack of sufficient TCW as shown in Fig. 13a. As the V_∞ increases beyond 10 km/s, the aerobraking mass fraction falls off sharply and becomes prohibitively small beyond 12 km/s. Aerocapture, on the other hand, becomes feasible for V_∞ of 12 km/s or more, and does reduce with increasing V_∞ but much less sharply than that for aerobraking. For V_∞ of 12 km/s, aerocapture delivers 79% more mass compared to aerobraking. The caveat mentioned in the case of Uranus, for the L/D requirement of 0.6–0.8 with the V_∞ of 12 km/s and the entry vehicle mass fractions used not being applicable, also applies here. For V_∞ of 16 km/s or higher, blunt-body aeroshells are viable and offer sufficient TCW. For V_∞ of 16 km/s, aerocapture delivers 424% more mass compared to aerobraking, and it is an enabling technology for Neptune mission as the propulsive and aerobraking payload mass fractions are prohibitively low. For V_∞ of 20 km/s or higher, aerocapture is the only feasible orbit insertion technique for missions to Neptune.

As seen in the case of Titan and Uranus, high-V_∞ trajectories using aerocapture can enable flight times to be as short as 7 years for missions to Neptune. In addition, the high V_∞ trajectories (15–20 km/s) can lower the vehicle L/D requirement to about 0.3–0.4, which is within the capability of blunt-body aeroshells. Additional study is recommended to characterize the aerothermodynamic environment encountered by aerocapture vehicles at such high entry speeds, and to validate the TPS mass fraction estimates used in this study. In addition to the savings in flight time compared to propulsive architectures, the substantial mass benefit offered by aerocapture will enable a well-instrumented spacecraft with additional elements such as a Triton lander to be accommodated in a future mission to the Neptune system.

VI. Comparative Studies

Figure 15 shows the range of typical entry speeds and the aerocapture corridor for lift and drag modulation control techniques at various destinations. Table 7 shows the range of interplanetary arrival V_∞ considered in the analysis for the various destinations. Venus and Earth show relatively similar entry conditions due to their similarity in size and gravity. At Mars, the entry speeds are smaller than that at

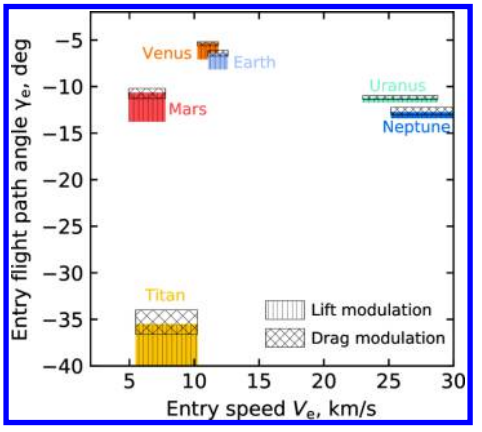

Fig. 15 Comparison of planet-relative entry speed and entry corridor for aerocapture at various targets for a vehicle with $L/D = 0.30$ for lift modulation and $\beta_2/\beta_1 = 7$ for drag modulation.

Table 7 Range of arrival V_∞ considered for various targets

Planet or moon	Range of V_∞, km/s, used in Figs. 15 and 18	V_∞, km/s, used in Figs. 16,17, and 19
Venus	0–6	3.0
Earth	0–6	3.0
Mars	0–6	3.0
Titan	5–10	7.5
Jupiter	5–10	7.5
Saturn	5–10	7.5
Uranus	10–22	16
Neptune	10–22	16

Earth or Venus. Titan with its low gravity and extended atmosphere results in the steepest entry of any planetary destination for aerocapture. Aerocapture vehicles at Uranus and Neptune encounter planet relative entry speeds in the range of 20–30 km/s.

Jupiter and Saturn are not included in Fig. 15 because the entry speeds are much higher than encountered at the other planets. Figure 16 shows the aerocapture theoretical corridor width at various destinations for lift modulation ($L/D = 0.30$) and drag modulation ($\beta_2/\beta_1 = 7$). The target capture orbits are the same as listed in Table 4. The arrival V_∞ is the average of the minimum and maximum values listed in Table 7. Titan offers the largest aerocapture corridor in the solar system for both lift and drag modulation techniques, followed by Mars, Earth, and Venus. Uranus and Neptune have substantially smaller corridor widths, which is attributed to the highly elliptical target orbits considered (primarily driven by the need for moon flybys) in contrast to the low-circular orbits considered at the inner planets and Titan.

Figure 17 shows the peak deceleration during the maneuver at various targets for typical entry conditions. The arrival V_∞ is the average of the minimum and maximum values listed in Table 7. For most destinations, the peak g-load is below $6g$ for lift modulation and below $4g$ for drag modulation. The peak deceleration does not show a strong dependence on the destination. Figure 18 shows a relative comparison of the stagnation point heat rate and total heat load at the various targets and shows a clear destination dependence. Mars and Titan present the most benign targets with peak heat rates less than 200 $\mathrm{W/cm^2}$ and heat load less than 50 $\mathrm{kJ/cm^2}$, making them ideal targets for an initial aerocapture mission with minimal requirements on the TPS materials. Aerocapture at Venus and Earth presents heat rates in the range of several hundred watts per square centimeter, whereas Uranus and Neptune result in heat rates in the range of several thousand watts per square centimeter and heat loads in the range of hundreds of kilojoules per square centimeter. While the peak heat rate at Uranus and Neptune is within the capability of TPS materials such as HEEET, the large heat loads may result in substantial TPS mass fraction and needs additional study. Jupiter presents an extreme case with heat rates in the range of tens of thousands of watts per square centimeter and thousands of kilojoules per square centimeter total heat load well beyond the capability of any existing TPS materials.

Stagnation-point heat rate and stagnation pressure, important parameters for TPS material qualification as test facility constraints, often limit the combination of the two parameters that can be achieved. Figure 19 shows the variation of stagnation-point heat rate and stagnation pressure for lift modulation aerocapture ($L/D = 0.30$) trajectories at various targets. Note that these results in Fig. 19 are for a single interplanetary arrival V_∞. Titan and Mars offer the most benign conditions for aerocapture requiring TPS materials to be qualified at

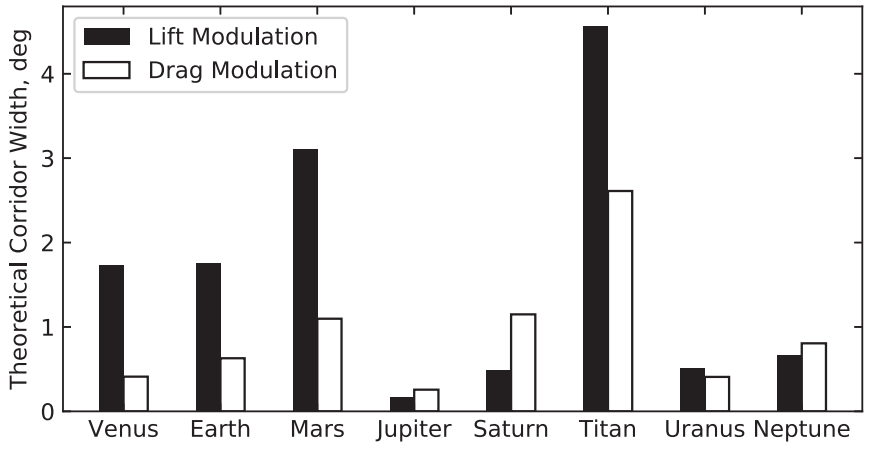

Fig. 16 Comparison of theoretical corridor width for aerocapture at various targets. $L/D = 0.30$ for lift modulation and $\beta_2/\beta_1 = 7$ for drag modulation.

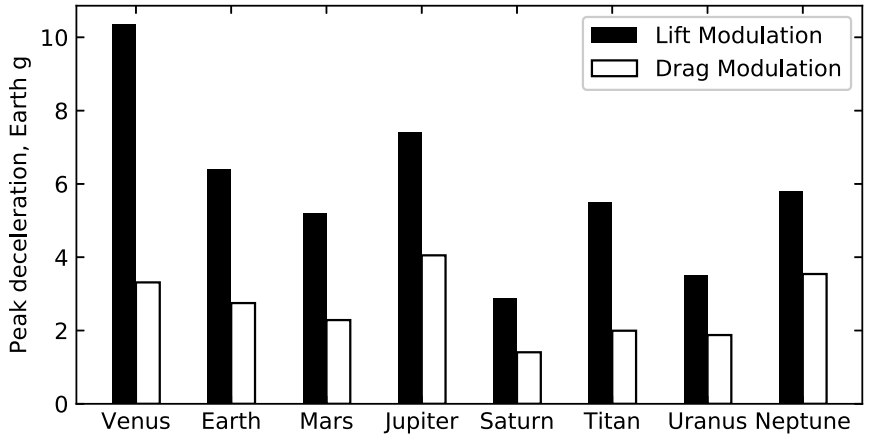

Fig. 17 Comparison of peak deceleration load for aerocapture at various targets. $L/D = 0.30$ for lift modulation and $\beta_2/\beta_1 = 7$ for drag modulation.

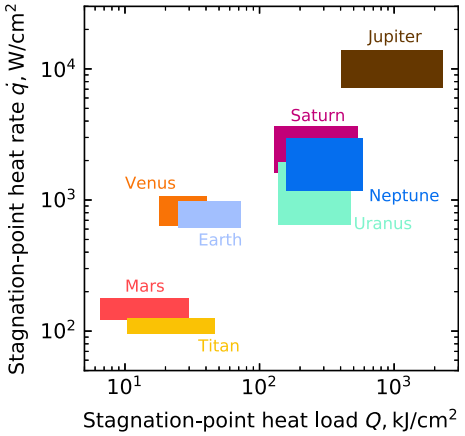

Fig. 18 Comparison of stagnation-point heat rate and total heat load for aerocapture at various targets. Results for a lift modulation vehicle with $L/D = 0.30$, and arrival V_∞ range listed in Table 7.

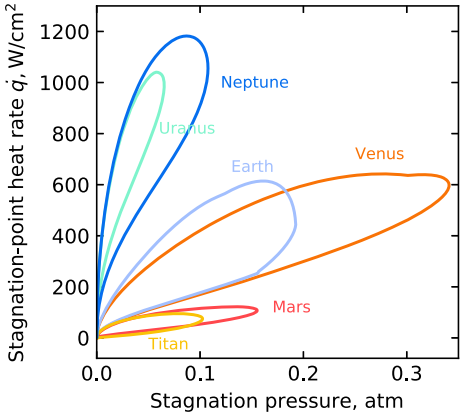

Fig. 19 Peak heat rate and stagnation pressure curves for lift modulation aerocapture ($L/D = 0.30$) at various targets. See Table 7 for arrival V_∞ used.

100–200W/cm^2 and 0.1–0.2 atm. Aerocapture at Venus requires the TPS material to accommodate several hundred watts per square centimeter at about 0.35 atm stagnation pressure. Aerocapture at Uranus and Neptune requires TPS materials to be qualified at a few thousand watts per square centimeter.

VII. Aerocapture Mission Analysis Tool (AMAT)

The lack of architectural tools and methods for high-level aerocapture mission design was identified by the NASA Ice Giants Pre-Decadal Study in 2017 [30] and Spilker et al. in 2018 [7]. Researchers at Purdue University have developed an open-source Python software package, the Aerocapture Mission Analysis Tool (AMAT), to fill this gap [45]. AMAT is designed to provide rapid mission analysis and trade study capabilities for aerocapture mission studies. AMAT supports aerocapture and entry, descent, and landing (EDL) mission analysis for all atmosphere-bearing destinations. AMAT can be accessed from the project homepage[‡‡] and provides numerous examples[§§] along with extensive documentation.[¶¶]

The high-level workflow for using AMAT in rapid mission studies is shown in Fig. 20. The mission designer defines a set of key vehicle parameters such as the ballistic coefficient along with acceptable constraint values such as TCW and peak heat rate. Based on these vehicle parameters, AMAT can be used to create aerocapture feasibility charts and determine if there is a feasible set of vehicle L/D (or β_2/β_1) and arrival V_∞. The mission designer also defines a baseline launch vehicle and high-level constraints such as launch mass and time of flight for the interplanetary trajectory. If there is a feasible set of trajectories that satisfy both the vehicle design and interplanetary trajectory constraints, a baseline vehicle design and trajectory is selected. Monte Carlo analysis is used to quantify orbit targeting accuracy and other parameters such as the peak heat rate in the presence of navigation and atmospheric uncertainties. If the vehicle performance is acceptable, the selected baseline design may be used as a starting point for higher-fidelity subsystem-level design and analysis. AMAT supports both lift and drag modulation control techniques and can be used for preliminary EDL analysis of atmospheric probes, landers, balloons, and rovers at any atmosphere-bearing destination.

[‡‡]https://github.com/athulpg007/AMAT.
[§§]https://github.com/athulpg007/AMAT/tree/master/examples.
[¶¶]https://amat.readthedocs.io.

VIII. Technology Readiness and Recommendations

Existing blunt-body aeroshells ($L/D < 0.35$) and TPS materials such as PICA are sufficient for aerocapture at Mars and Titan. In fact, an MSL-derived aeroshell ($L/D = 0.24$) could perform aerocapture at Mars and Titan with no new technology developments other than that related to spacecraft packaging, deployable antennae, and aeroshell jettison after the aerocapture maneuver. Such a system could also potentially be used at Venus, with some modifications to accommodate the higher heat rates and heat loads. Drag modulation aerocapture is also viable at Mars, Venus, and Titan with modest ballistic coefficient ratios ($\beta_2/\beta_1 < 7$), and proven carbon cloth or PICA TPS. Drag modulation aerocapture has the potential to enable a new paradigm in the exploration of Mars and Venus through small satellite constellations at these destinations within the next decade. Aerocapture at Earth is viable using existing aeroshells such as Orion, and it is a viable option for sample return and crewed missions returning from the Moon or Mars. Aerocapture at Uranus and Neptune has been shown to be possible using blunt-body aeroshells with L/D of 0.30–0.40 with improvements in interplanetary navigation and vehicle guidance techniques [5,29,31]. HEEET has already been tested under conditions relevant for aerocapture and is ready for mission infusion [90]. More detailed flight-system studies are likely required to establish a baseline design reference mission, and estimate the TPS mass fraction with better accuracy, which is currently not well known for Uranus and Neptune. With some additional studies to quantify the aerothermal environment and modest technological developments such as tailoring HEEET for a particular mission profile, aerocapture at Uranus and Neptune could be viable for a Flagship-class mission in the next decade. Aerocapture at Jupiter and Saturn is not viable using blunt-body aeroshells, well beyond the capability of existing TPS materials.

The present study recommends NASA support efforts to demonstrate drag modulation aerocapture at Earth using the small satellite mission concept proposed by Werner and Braun [36] leveraging a low-cost launch as secondary payload on a GTO mission. Dynamics of drag skirt separation and the risk of recontact of the skirt have been studied using CFD and ballistic range tests by Rollock and Braun [91] and by McClary and Putnam [92]. Austin et al. [1] have developed a reference drag modulation aerocapture flight system design using the drag skirt for use at Mars and Venus. The study recommends continued NASA support of these efforts to realize small, low-cost aerocapture missions potentially as secondary payloads on future Mars and Venus science missions. A low-cost demonstration mission at Earth or Mars will establish flight heritage for aerocapture in the near-term and lower the risk for larger science missions.

The study recommends continued development of the HEEET TPS particularly tailoring the material layup for the aerothermal conditions encountered at Uranus and Neptune, and more detailed aerothermodynamic studies to estimate the TPS mass fraction for aerocapture at the outer planets. Probe delivery along with aerocapture at the outer planets is a topic of current research [93], and additional studies are required to establish a baseline aerocapture mission architecture with a probe delivery at Uranus and Neptune for a future Flagship-class mission. Other technologies relevant to outer planet aerocapture include autonomous spacecraft navigation, improved flight control techniques and guidance schemes, spacecraft autonomy (automatically determine orbit and perform corrective

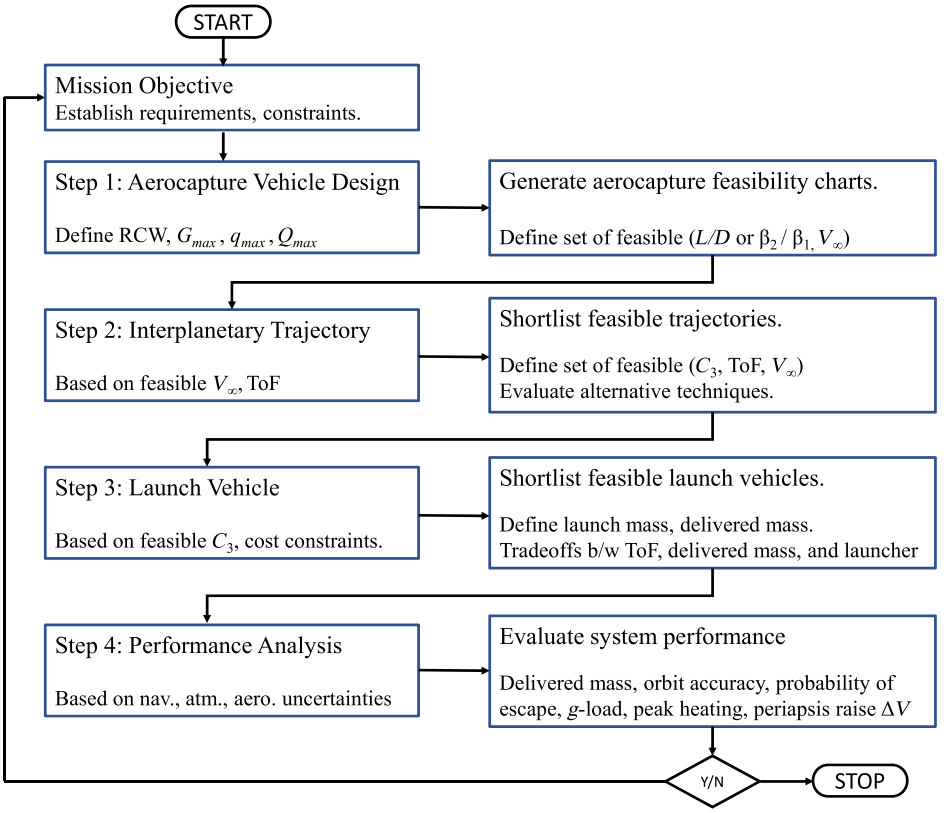

Fig. 20 AMAT rapid mission design workflow.

maneuvers after aerocapture without ground intervention), and spacecraft packaging inside the aeroshell. The study recommends continued NASA support for GRAM model development, especially for Uranus and Neptune for which our knowledge is most lacking. Opportunistic stellar occultations and ground-based observations can help improve our understanding of these atmospheres [7,94]. Further development of AMAT and other aerocapture design tools is required to provide higher-fidelity aeroshell mass estimates, particularly for outer planet missions.

IX. Summary

The present study performed a quantitative and comparative assessment of the feasibility of aerocapture at all atmosphere-bearing solar system destinations. Aerocapture feasibility charts are used to concisely present the various constraints arising from corridor width, deceleration, and heating constraints for both lift and drag modulation control techniques. Results indicate that existing heritage blunt-body aeroshells ($L/D < 0.30$) and flight-proven TPS materials are sufficient for lift modulation aerocapture at Venus, Earth, Mars, and Titan. Drag modulation aerocapture at these destinations is also viable using modest ballistic coefficient ratios ($\beta_2/\beta_1 < 7$), making them an attractive choice for inserting small satellites into orbit. Aerocapture at Uranus and Neptune is viable with blunt-body aeroshells (L/D of 0.30–0.40) with certain high arrival V_∞ interplanetary trajectories and improved guidance schemes. The mass benefit offered by lift modulation aerocapture is compared against purely propulsive insertion and aerobraking at the various planetary destinations. For Venus and Mars, aerobraking outperforms aerocapture for low arrival V_∞ (<5 km/s) and is the preferred orbit insertion method. For interplanetary trajectories with higher arrival V_∞, aerocapture delivers 100–200% more mass to Venus and 100–400% more mass to Mars. For Titan, aerocapture can deliver more than 300% more mass along with lower interplanetary flight times. At Uranus and Neptune, aerocapture can deliver as much as 600 and 400% more mass, respectively, and shorten flight times by 5 and 7 years, respectively. Comparing the aerothermal conditions encountered during aerocapture, Mars and Titan offer the most benign entry environments, whereas Jupiter and Saturn present the most extreme conditions. Aerocapture at Jupiter is not viable in the near-term due to the extreme aerothermal entry conditions at these planets. A new open-source software, the Aerocapture Mission Analysis Tool, has been developed to aid rapid conceptual design of aerocapture missions considering both interplanetary trajectory and vehicle design aspects. The study reviewed the technology readiness of aerocapture for various destinations and provides recommendations for flight experiments and technology developments.

X. Conclusions

Aerocapture has been shown to be feasible at Mars, Titan, and Venus with existing vehicle designs for both lift modulation and drag modulation control techniques and flight-proven TPS materials. Aerocapture at Uranus and Neptune is shown to be viable with lifting vehicles with L/D of 0.30–0.40 with the use of high arrival V_∞ interplanetary trajectories, improvements in interplanetary navigation, and vehicle guidance schemes. Although the aerothermal loads at Uranus and Neptune are substantially larger than that at Mars or Titan, it is within the limits of HEEET TPS that has been laboratory-tested under comparable conditions. Additional studies are required to evaluate the feasibility of drag modulation systems at Uranus and Neptune considering the more demanding aerothermal conditions at these destinations. Aerocapture at Jupiter and Saturn is not feasible using existing vehicle designs and will require significant advances over existing TPS materials. Aerocapture is shown to provide enhancing capability for missions to Venus (100–200% more delivered mass) and Mars (100–400%) with high arrival V_∞ interplanetary trajectories. For missions to Titan, aerocapture is strongly enhancing (300–1700% more mass) for interplanetary trajectories with arrival V_∞ from 6 to 8 km/s and is an enabling technology for higher arrival V_∞ trajectories. For missions to Uranus, aerocapture is strongly enhancing (100–600%) for V_∞ from 12 to 16 km/s and enabling for arrival V_∞ beyond 16 km/s. For missions to Neptune, aerocapture delivers 80–400% more mass for interplanetary trajectories with V_∞

from 12 to 16 km/s and is an enabling technology for higher arrival V_∞. High-arrival-V_∞ trajectories ($V_\infty > 16$ km/s) can potentially allow interplanetary flight times to be as low as 6 and 8 years to Uranus and Neptune, respectively. A low-cost technology demonstration mission at Earth or Mars can establish flight heritage for aerocapture and lower the risk posture for larger science missions. As pointed out by Spilker et al. [7], the benefits offered by aerocapture for future missions could be compared to the vastly increased capability for exploration offered by the gravity-assist technique in the early days of interplanetary flight. Once proven, aerocapture could be a key strategy enabling large constellations of small satellites around Mars and Venus and delivering sizeable orbiters within reasonable flight times to the outer solar system.

Appendix: Additional Aerocapture Feasibility Charts

A. Venus

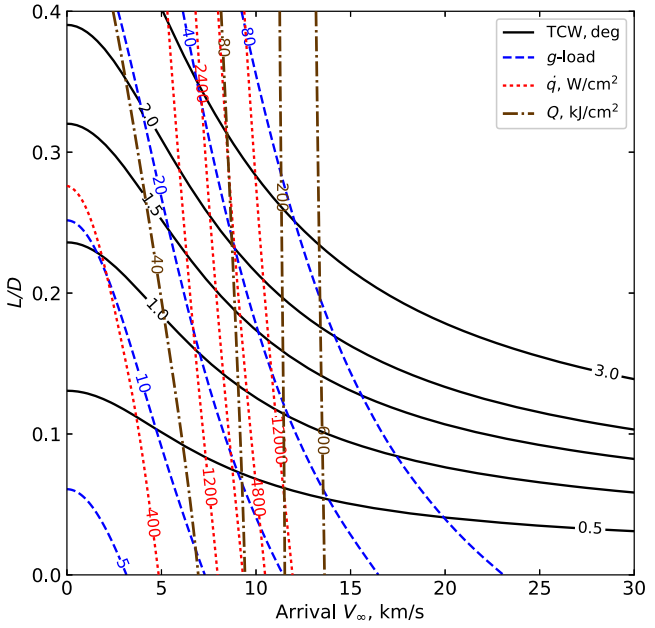

Fig. A1 Lift modulation aerocapture feasibility chart for Venus. $\beta = 200$ kg/m^2; $R_N = 1.0$ m.

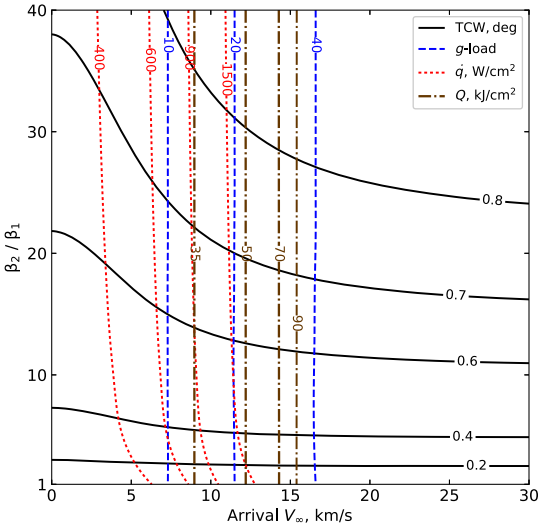

Fig. A2 Drag modulation aerocapture feasibility chart for Venus. $\beta_1 = 20$ kg/m^2; $R_N = 0.1$ m.

B. Earth

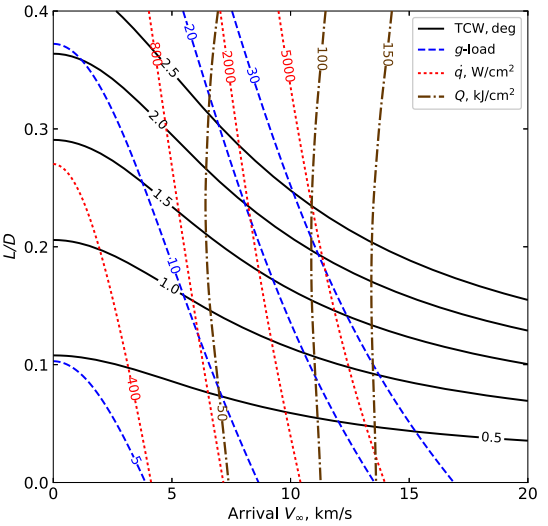

Fig. B1 Lift modulation aerocapture feasibility chart for Earth. $\beta = 200$ kg/m^2; $R_N = 1.0$ m.

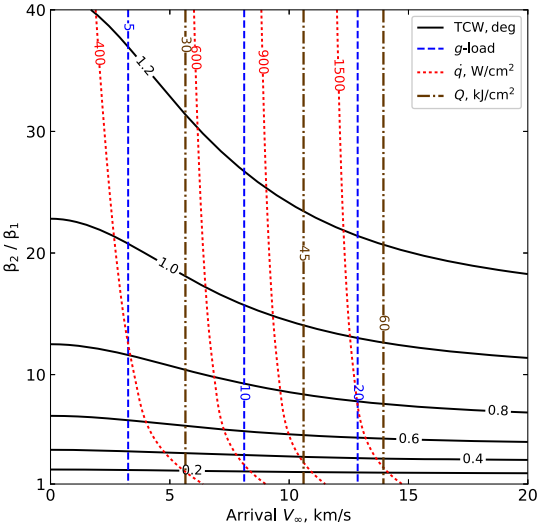

Fig. B2 Drag modulation aerocapture feasibility chart for Earth. $\beta_1 = 20$ kg/m^2; $R_N = 0.1$ m.

C. Mars

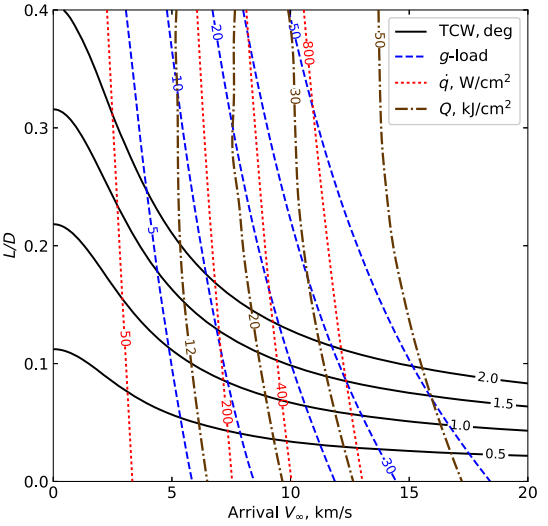

Fig. C1 Lift modulation aerocapture feasibility chart for Mars. $\beta = 200$ kg/m^2; $R_N = 1.0$ m.

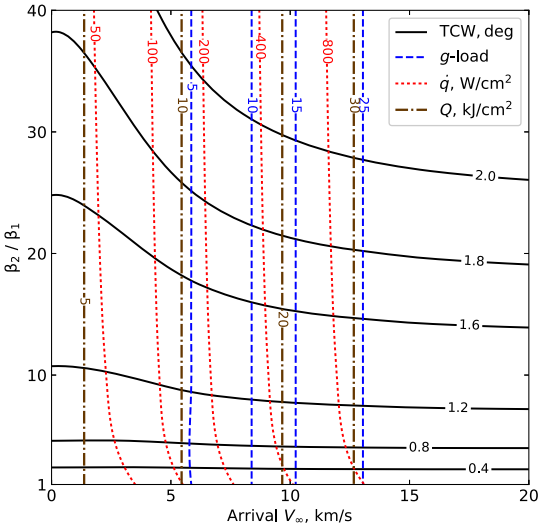

Fig. C2 Drag modulation aerocapture feasibility chart for Mars. $\beta_1 = 20$ kg/m^2; $R_N = 0.1$ m.

D. Jupiter

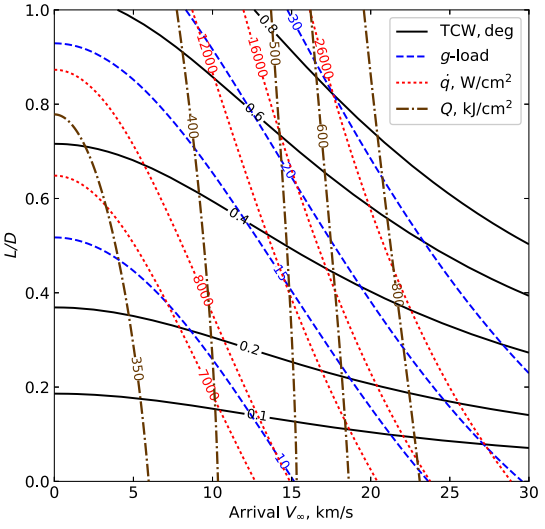

Fig. D1 Lift modulation aerocapture feasibility chart for Jupiter. $\beta = 200$ kg/m^2; $R_N = 1.0$ m.

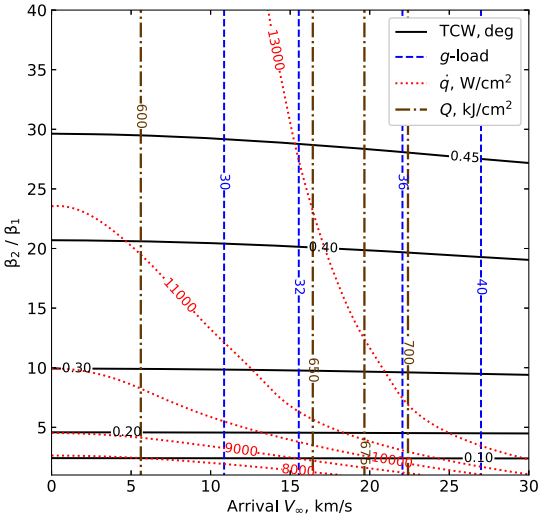

Fig. D2 Drag modulation aerocapture feasibility chart for Jupiter. $\beta_1 = 20$ kg/m^2; $R_N = 0.1$ m.

E. Saturn

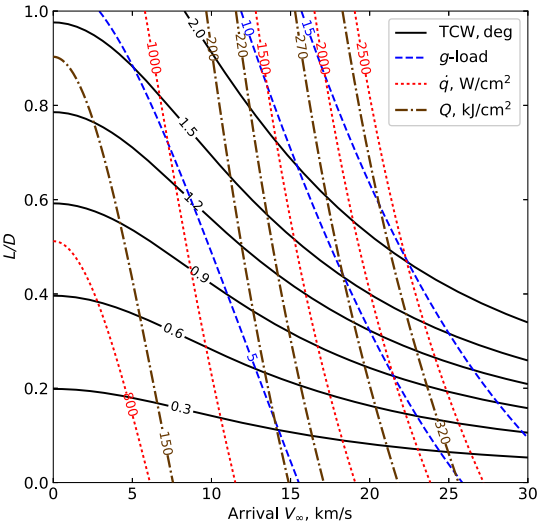

Fig. E1 Lift modulation aerocapture feasibility chart for Saturn. $\beta = 200$ kg/m^2; $R_N = 1.0$ m.

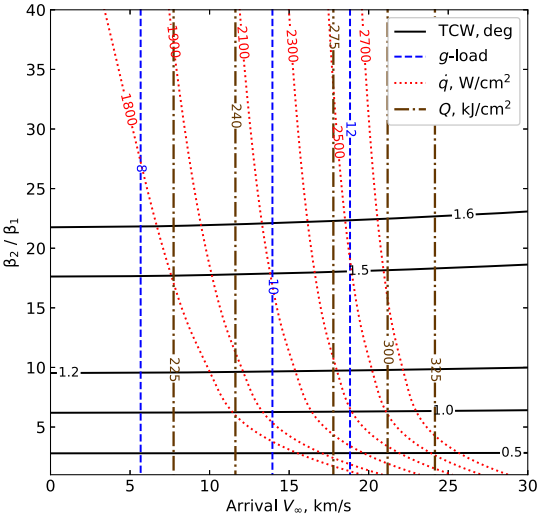

Fig. E2 Drag modulation aerocapture feasibility chart for Saturn. $\beta_1 = 20$ kg/m^2; $R_N = 0.1$ m.

F. Titan

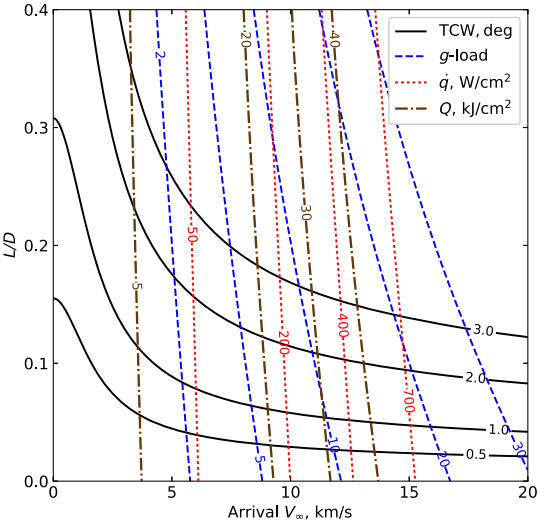

Fig. F1 Lift modulation aerocapture feasibility chart for Titan. $\beta = 200$ kg/m^2; $R_N = 1.0$ m.

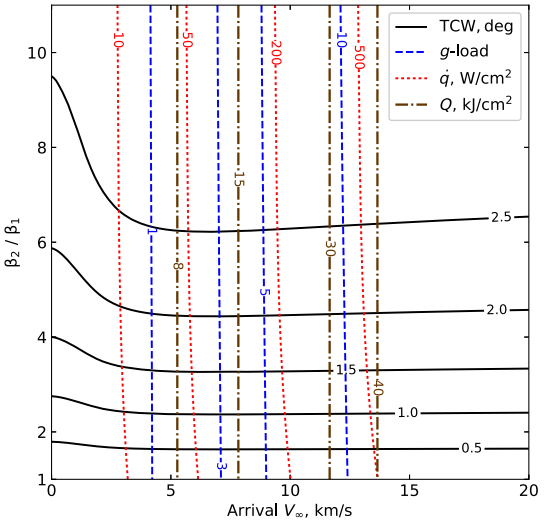

Fig. F2 Drag modulation aerocapture feasibility chart for Titan. $\beta_1 = 20$ kg/m^2; $R_N = 0.1$ m.

G. Uranus

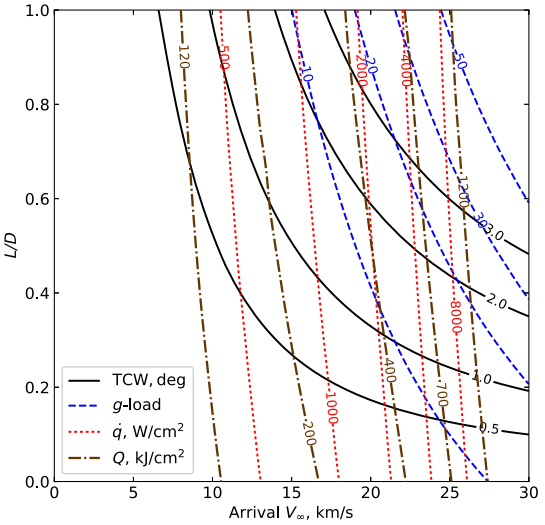

Fig. G1 Lift modulation aerocapture feasibility chart for Uranus. $\beta = 200$ kg/m^2; $R_N = 1.0$ m.

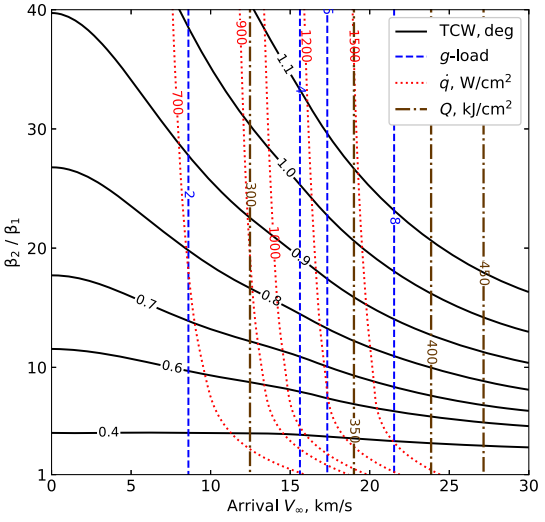

Fig. G2 Drag modulation aerocapture feasibility chart for Uranus. $\beta_1 = 20$ kg/m^2; $R_N = 0.1$ m.

H. Neptune

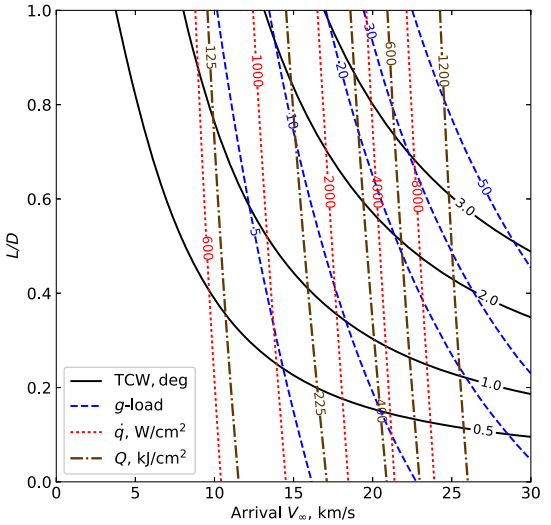

Fig. H1 Lift modulation aerocapture feasibility chart for Neptune. $\beta = 200$ kg/m^2; $R_N = 0.1$ m.

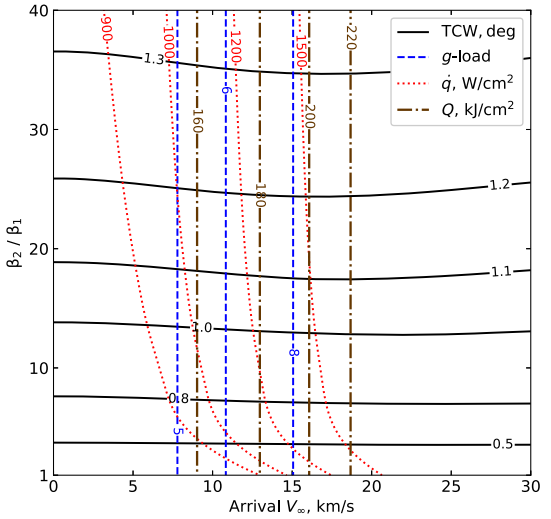

Fig. H2 Drag modulation aerocapture feasibility chart for Neptune. $\beta_1 = 20$ kg/m^2; $R_N = 0.1$ m.

Supplemental Data

All the figures in the paper were created using AMAT. Jupyter Notebooks to perform the analysis in the paper are available online at the AMAT documentation website (https://amat.readthedocs.io/en/master/jsr-notebooks.html) and can be downloaded from the AMAT GitHub repository (https://github.com/athulpg007/AMAT/tree/master/examples/jsr-notebooks).

Acknowledgments

The authors acknowledge Alec Mudek at Purdue University for generating Earth–Venus trajectory data using STOUR. The authors acknowledge Anastassios Petropoulos at the NASA Jet Propulsion Laboratory and Nitin Arora formerly at the NASA Jet Propulsion Laboratory for providing the interplanetary trajectory data for Uranus and Neptune. The authors acknowledge Alex Austin at the NASA Jet Propulsion Laboratory and Soumyo Dutta at the NASA Langley Research Center for many helpful discussions related to various ongoing aerocapture technology development efforts.

References

[1] Austin, A., Nelessen, A., Strauss, B., Ravich, J., Jesick, M., Venkatapathy, E., Beck, R., Wercinski, P., Aftosmis, M., Wilder, M., Allen, G., Braun, R., Werner, M., and Roelke, E., "SmallSat Aerocapture to Enable a New Paradigm of Planetary Missions," *2019 IEEE Aerospace Conference*, Inst. of Electrical and Electronics Engineers, New York, 2019, pp. 1–20.
https://doi.org/10.1109/AERO.2019.8742220

[2] Falcone, G., Williams, J., and Putnam, Z., "Assessment of Aerocapture for Orbit Insertion of Small Satellites at Mars," *Journal of Spacecraft and Rockets*, Vol. 56, No. 6, 2019, pp. 1689–1703.
https://doi.org/10.2514/1.A34444

[3] Girija, A. P., Lu, Y., and Saikia, S. J., "Feasibility and Mass-Benefit Analysis of Aerocapture for Missions to Venus," *Journal of Spacecraft and Rockets*, Vol. 57, No. 1, 2020, pp. 58–73.
https://doi.org/10.2514/1.A34529

[4] Lockwood, M. K., Starr, B. R., Paulson, J. W., Jr., Kontinos, D. A., Chen, Y., Laub, B., Olejniczak, J., Wright, M. J., Takashima, N., and Justus, C. G., "Systems Analysis for a Venus Aerocapture Mission," NASA TM-2006-214291, 2006, https://ntrs.nasa.gov/archive/nasa/casi.ntrs.nasa.gov/20060010899.pdf.

[5] Girija, A. P., Saikia, S. J., Longuski, J. M., Bhaskaran, S., Smith, M. S., and Cutts, J. A., "Feasibility and Performance Analysis of Neptune Aerocapture Using Heritage Blunt-Body Aeroshells," *Journal of Spacecraft and Rockets*, Vol. 57, No. 6, 2020, pp. 1186–1203.
https://doi.org/10.2514/1.A34719

[6] Dutta, S., Perez-Ayucar, M., Fedele, A., Gardi, R., Calabuig, G. D., Schuster, S., Lebreton, J.-P., Ali, H. K., Sayanagi, K., Sakraker Ozmen, I., et al., "Aerocapture as an Enhancing Option for Ice Giants Missions," *Bulletin of the American Astronomical Society*, Vol. 53, No. 4, 2021, p. 46.
https://doi.org/10.3847/25c2cfeb.e8e49d0e

[7] Spilker, T. R., Adler, M., Arora, N., Beauchamp, P. M., Cutts, J. A., Munk, M. M., Powell, R. W., Braun, R. D., and Wercinski, P. F., "Qualitative Assessment of Aerocapture and Applications to Future Missions," *Journal of Spacecraft and Rockets*, Vol. 56, No. 2, 2018, pp. 536–545.
https://doi.org/10.2514/1.A34056

[8] London, H. S., "Change of Satellite Orbit Plane by Aerodynamic Maneuvering," *Journal of the Aerospace Sciences*, Vol. 29, No. 3, 1962, pp. 323–332.
https://doi.org/10.2514/8.9416

[9] Repic, E. M., Boobar, G. M., and Chapel, F. G., "Aerobraking as a Potential Planetary Capture Mode," *Journal of Spacecraft and Rockets*, Vol. 5, No. 8, 1968, pp. 921–926.
https://doi.org/10.2514/3.29389

[10] Finch, T. W., "Aerodynamic Braking Trajectories for Mars Orbit Attainment," *Journal of Spacecraft and Rockets*, Vol. 2, No. 4, 1965, pp. 497–500.
https://doi.org/10.2514/3.28218

[11] Lichtenstein, J. H., "Some Considerations on the Use of Atmospheric Braking for a Transfer Into a Martian Orbit," NASA TN D-2837, 1965.

[12] Cruz, M., "The Aerocapture Vehicle Mission Design Concept," *Conference on Advanced Technology for Future Space Systems*, AIAA, Reston, VA, 1979, pp. 1–893.
https://doi.org/10.2514/6.1979-893

[13] Cruz, M., "Technology Requirements for a Generic Aerocapture System," *15th Thermophysics Conference*, AIAA Paper 1980-1493, 1980.
https://doi.org/10.2514/6.1980-1493

[14] Cruz, M., "Aerodynamic Mission Concepts for the Mars Sample Return Mission," *7th Atmospheric Flight Mechanics Conference*, AIAA Paper 1981-1859, 1981.
https://doi.org/10.2514/6.1981-1859

[15] Carpenter, R., "Aeroasist Flight Experiment," Texas Space Grant Consortium TR ASE 396, Austin, TX, 1992, http://www.tsgc.utexas.edu/archive/PDF/AeroassistFlightExp.pdf.

[16] Papadopoulos, P., Venkatapathy, E., Henline, W., Wercinski, P., and Papadopoulos, P., "Aerothermal Heating Simulations with Surface Catalysis for the Mars 2001 Aerocapture Mission," *35th Aerospace Sciences Meeting and Exhibit*, AIAA Paper 1997-0473, 1997.
https://doi.org/10.2514/6.1997-473

[17] Cazaux, C., Naderi, F., Whetsel, C., Beaty, D., Gershman, B., Kornfeld, R., Mitcheltree, B., and Sackheim, B., "The NASA/CNES Mars Sample Return–A Status Report," *Acta Astronautica*, Vol. 54, No. 8, 2004, pp. 601–617.
https://doi.org/10.1016/j.actaastro.2003.07.001

[18] Hall, J., "An Overview of the ST-7 Aerocapture Flight Test Experiment," *AIAA Atmospheric Flight Mechanics Conference and Exhibit*, AIAA Paper 2002-4621, 2002.
https://doi.org/10.2514/6.2002-4621

[19] Keys, A., Hall, J., Oh, D., and Munk, M., "Overview of a Proposed Flight Validation of Aerocapture System Technology for Planetary Missions," *42nd AIAA/ASME/SAE/ASEE Joint Propulsion Conference & Exhibit*, AIAA Paper 2006-4518, 2006.
https://doi.org/10.2514/6.2006-4518

[20] James, B., and Munk, M., "Aerocapture Technology Development Within the NASA In-Space Propulsion Program," *39th AIAA/ASME/SAE/ASEE Joint Propulsion Conference and Exhibit*, AIAA Paper 2003-4654, 2003.
https://doi.org/10.2514/6.2003-4654

[21] Wright, H. S., Oh, D. Y., Westhelle, C. H., Fisher, J. L., Dyke, R. E., Edquist, K. T., Brown, J. L., Justh, H. L., and Munk, M. M., "Mars Aerocapture Systems Study," NASA TM-2006-214522, 2006, https://ntrs.nasa.gov/archive/nasa/casi.ntrs.nasa.gov/20060056070.pdf.

[22] Lockwood, M. K., Queen, E. M., Way, D. W., Powell, R. W., Edquist, K., Starr, B. W., Hollis, B. R., Zoby, E. V., Hrinda, G. A., and Bailey, R. W., "Aerocapture Systems Analysis for a Titan Mission," NASA TM-2006-214273, 2006, https://ntrs.nasa.gov/archive/nasa/casi.ntrs.nasa.gov/20060007561.pdf.

[23] Lockwood, M. K., Edquist, K. T., Starr, B. R., Hollis, B. R., Hrinda, G. A., Bailey, R. W., Hall, J. L., Spilker, T. R., Noca, M. A., and O'Kongo, N., "Aerocapture Systems Analysis for a Neptune Mission," NASA TM-2006-214300, 2006, https://ntrs.nasa.gov/archive/nasa/casi.ntrs.nasa.gov/20060012088.pdf.

[24] Artis, G., and James, B., "Aerocapture Technology to Reduce Trip Time and Cost of Planetary Missions," *AAS/Division for Planetary Sciences Meeting*, American Astronomical Society, Washington, D.C., Oct. 2006.

[25] Hall, J. L., Noca, M. A., and Bailey, R. W., "Cost-Benefit Analysis of the Aerocapture Mission Set," *Journal of Spacecraft and Rockets*, Vol. 42, No. 2, 2005, pp. 309–320.
https://doi.org/10.2514/1.4118

[26] Ingersoll, A. P., and Spilker, T. R., "A Neptune Orbiter with Probes Mission with Aerocapture Orbit Insertion," *Progress in Astronautics and Aeronautics: NASA Space Science Vision Missions*, Vol. 224, 2008, pp. 81–113.
https://doi.org/10.2514/5.9781600866920.0081.0114

[27] Fujita, K., and Narita, S., "Conceptual Study of a Small-Sized Mars Aerocapture Demonstrator," *51st AIAA Aerospace Sciences Meeting Including the New Horizons Forum and Aerospace Exposition*, AIAA Paper 2013-0729, 2013.
https://doi.org/10.2514/6.2013-729

[28] Putnam, Z. R., and Braun, R. D., "Drag-Modulation Flight-Control System Options for Planetary Aerocapture," *Journal of Spacecraft and Rockets*, Vol. 51, No. 1, 2013, pp. 139–150.
https://doi.org/10.2514/1.A32589

[29] Saikia, S. J., Millane, J., Lu, Y., Mudek, A., Arora, A., Witsberge, P., Hughes, K., Longuski, J. M., Spilker, T., Petropoulos, A., Arora, N., Cutts, J., Elliott, J., Sims, J., and Reh, K., "Aerocapture Assessment for NASA Ice Giants Pre-Decadal Survey Mission Study," *Journal of Spacecraft and Rockets*, Vol. 58, No. 2, 2021, pp. 1–11.
https://doi.org/10.2514/1.A34703

[30] Hofstadter, M. D., Simon, A., Reh, K., and Elliot, J., "Ice Giants Pre-Decadal Study Final Report," NASA JPL D-100520, Pasadena, CA, 2017, https://www.lpi.usra.edu/icegiants/mission_study/.

[31] Deshmukh, R. G., Spencer, D. A., and Dutta, S., "Investigation of Direct Force Control for Aerocapture at Neptune," *Acta Astronautica*, Vol. 175, Oct. 2020, pp. 375–386.
https://doi.org/10.1016/j.actaastro.2020.05.047

[32] Heidrich, C., Dutta, S., and Braun, R., "Modern Aerocapture Guidance to Enable Reduced-Lift Vehicles at Neptune," *AAS/AIAA Astrodynamics Specialist Conference*, AAS Paper 19-221, Portland, ME, 2019.

[33] Ramsey, P., and Lyne, J. E., "Investigation of Titan Aerogravity Assist for Capture into Orbit About Saturn," *Journal of Spacecraft and Rockets*, Vol. 43, No. 1, 2006, pp. 231–233.
https://doi.org/10.2514/1.9274

[34] Randolph, J. E., and McRonald, A. D., "Solar System Fast Mission Trajectories Using Aerogravity Assist," *Journal of spacecraft and rockets*, Vol. 29, No. 2, 1992, pp. 223–232.
https://doi.org/10.2514/3.26338

[35] Lu, Y., and Saikia, S. J., "Titan Aerogravity-Assist Maneuvers for Saturn/Enceladus Missions," *Acta Astronautica*, Vol. 176, Nov. 2020, pp. 262–275.
https://doi.org/10.1016/j.actaastro.2020.06.001

[36] Werner, M. S., and Braun, R. D., "Mission Design and Performance Analysis of a Smallsat Aerocapture Flight Test," *Journal of Spacecraft and Rockets*, Vol. 56, No. 6, 2019, pp. 1704–1713. https://doi.org/10.2514/1.A33997

[37] Nelessen, A., Austin, A., Ravich, J., Strauss, B., Venkatapathy, E., Beck, R., Wercinski, P., Wilder, M., Allen, G., Aftomis, M., Braun, R., Werner, M., and Roelke, E., "Small Satellite Aerocapture for Increased Mass Delivered to Venus and Beyond," *15th International Planetary Probe Workshop*, IPPW, Boulder, CO, 2018, https://www.colorado.edu/event/ippw2018/sites/default/files/attached-files/smallprobes_1_nelessen_presid622_presslides_docid1143.pdf.

[38] Roelke, E., Werner, M., and Braun, R. D., "Single-Stage Drag Modulation GNC Performance for Venus Aerocapture Demonstration," *AIAA Scitech 2019 Forum*, AIAA Paper 2019-0016, 2019. https://doi.org/10.2514/6.2019-0016

[39] Roelke, E., and Braun, R., "Discrete-Event Drag-Modulated Guidance Performance for Venus Aerocapture," *Journal of Spacecraft and Rockets*, Vol. 58, No. 1, 2021, pp. 190–199. https://doi.org/10.2514/1.A34761

[40] Deshmukh, R., Cabrera, J. V., and Spencer, D., "SmallSat Aerocapture using a Generalized Numerical Predictor Corrector Guidance Architecture," *AIAA Scitech 2021 Forum*, AIAA Paper 2021-1066, 2021. https://doi.org/10.2514/6.2021-1066

[41] Roelke, E., McMahon, J. W., Braun, R. D., and Hattis, P. D., "Multi-Event Jettison Guidance Approaches for Drag-Modulation Aerocapture," *2020 AAS/AIAA Astrodynamics Specialist Conference*, American Astronautical Society, Springfield, VA, Aug. 2020, pp. 1–13 (Article in Advance). https://doi.org/10.2514/1.A35059

[42] Mercer, C., "Planetary Science Deep Space SmallSat Studies," *48th Lunar Planetary Science Conference Special Session*, Lunar and Planetary Inst., Houston, TX, 2018.

[43] Girija, A. P., "A Systems Framework and Analysis Tool for Rapid Conceptual Design of Aerocapture Missions," Ph.D. Thesis, Purdue Univ., West Lafayette, IN, 2021. https://doi.org/10.25394/PGS.14903349.v1

[44] Lu, Y., and Saikia, S. J., "Feasibility Assessment of Aerocapture for Future Titan Orbiter Missions," *Journal of Spacecraft and Rockets*, Vol. 55, No. 5, 2018, pp. 1125–1135. https://doi.org/10.2514/1.A34121

[45] Girija, A. P., Saikia, S. J., Longuski, J. M., and Cutts, J. A., "AMAT: A Python Package for Rapid Conceptual Design of Aerocapture and Atmospheric Entry, Descent, and Landing (EDL) Missions in a Jupyter Environment," *Journal of Open Source Software*, Vol. 6, No. 67, 2021, p. 3710. https://doi.org/10.21105/joss.03710

[46] Haw, R. J., Bhaskaran, S., Strauss, W., Sklyanskiy, E., Graat, E., Smith, J., Menom, P., Ardalan, S., Ballard, C., Williams, P., Kawaguchi, J., Makoto, Y., and Ohnishi, T., "Hayabusa: Navigation Challenges for Earth Return," Jet Propulsion Lab. JPL-TRS-43827, 2011, https://trs.jpl.nasa.gov/handle/2014/43827.

[47] Martin-Mur, T., Kruizinga, G., Burkhart, P., Abilleira, F., Wong, M., and Kangas, J., "Mars Science Laboratory Interplanetary Navigation," *Journal of Spacecraft and Rockets*, Vol. 51, No. 4, 2014, pp. 1014–1028. https://doi.org/10.2514/1.A32631

[48] Way, D., Powell, R., Masciarelli, J., Starr, B., and Edquist, K., "Aerocapture Simulation and Performance for the Titan Explorer Mission," *39th AIAA/ASME/SAE/ASEE Joint Propulsion Conference and Exhibit*, AIAA Paper 2003-4951, 2003. https://doi.org/10.2514/6.2003-4951

[49] Starr, B., Westhelle, C., and Masciarelli, J., "Aerocapture Performance Analysis for a Neptune-Triton Exploration Mission," *AIAA Atmospheric Flight Mechanics Conference and Exhibit*, AIAA Paper 2004-4955, 2004. https://doi.org/10.2514/6.2004-4955

[50] Sutton, K., and Graves, R. A., Jr., "A General Stagnation-Point Convective Heating Equation for Arbitrary Gas Mixtures," NASA TR-R-376, 1971, https://ntrs.nasa.gov/archive/nasa/casi.ntrs.nasa.gov/19720003329.pdf.

[51] Samareh, J. A., "A Multidisciplinary Tool for Systems Analysis of Planetary Entry, Descent, and Landing (SAPE)," NASA TM-2009-215950, 2009, https://ntrs.nasa.gov/archive/nasa/casi.ntrs.nasa.gov/20090041828.pdf.

[52] Craig, S., and Lyne, J. E., "Parametric Study of Aerocapture for Missions to Venus," *Journal of Spacecraft and Rockets*, Vol. 42, No. 6, 2005, pp. 1035–1038. https://doi.org/10.2514/1.2589

[53] Johnson, S. M., "Thermal Protection Materials and Systems: Past, Present, and Future," NASA Ames Research Center ARC-E-DAA-TN9472, 2013, https://ntrs.nasa.gov/archive/nasa/casi.ntrs.nasa.gov/20130014035.pdf.

[54] Covington, M., "Performance of a Light-Weight Ablative Thermal Protection Material for the Stardust Mission Sample Return Capsule," Eloret Corp., NASA CP-2004-213456, 2005.

[55] Ellerby, D., Driver, D., Gasch, M., Mahzari, M., Milos, F., Owen, N., Peterson, K., Stackpoole, M., Venkatapathy, E., and Young, Z., "Overview of Heatshield for Extreme Entry Environment Technology (HEEET) Project," *16th International Planetary Probe Workshop (IPPW)*, Univ. of Colorado, Boulder, June 2018, https://www.colorado.edu/event/ippw2018/sites/default/files/attached-files/aeroentrytech_7_ellerby_presid594_presslides_docid1160.pdf.

[56] Brandis, A. M., and Johnston, C. O., "Characterization of Stagnation-point Heat Flux for Earth Entry," *45th AIAA Plasmadynamics and Lasers Conference*, AIAA Paper 2014-2374, 2014. https://doi.org/10.2514/6.2014-2374

[57] Ritter, H., Mazoué, F., Santovincenzo, A., and Atzei, A., "Jupiter Entry Probe Feasibility Study from the ESTEC CDF Team: Heat Flux Evaluation and TPS Definition," *5th European Workshop on Thermal Protection Systems and Hot Structures*, Vol. 631, European Space Agency, Noordwijk, The Netherlands, 2006.

[58] Bienstock, B., Atkinson, D., Atreya, S., Mahaffy, P., Baines, K., Wright, M., Wright, M., Stern, A., Steffes, P., Smith, D., Frampton, R., Peltz, L., Sichi, S., Masciarelli, J., Van Cleve, J., Murrow, D., and Landin, B., "NASA Vision Mission Neptune Orbiter with Probes," NASA Contract No. NNH04CC41C, 2005.

[59] Olejniczak, J., Prabhu, D., Wright, M., Takashima, N., Hollis, B., Sutton, K., and Zoby, E., "An Analysis of the Radiative Heating Environment for Aerocapture at Titan," *39th AIAA/ASME/SAE/ASEE Joint Propulsion Conference and Exhibit*, AIAA Paper 2003-4953, 2003. https://doi.org/10.2514/6.2003-4953

[60] Wright, M. J., Bose, D., and Olejniczak, J., "Impact of Flowfield-Radiation Coupling on Aeroheating for Titan Aerocapture," *Journal of Thermophysics and Heat Transfer*, Vol. 19, No. 1, 2005, pp. 17–27. https://doi.org/10.2514/1.10304

[61] Dutta, S., Smith, B., Prabhu, D., and Venkatapathy, E., "Mission Sizing and Trade Studies for Low Ballistic Coefficient Entry Systems to Venus," *2012 IEEE Aerospace Conference*, Inst. of Electrical and Electronics Engineers, New York, 2012, pp. 1–14. https://doi.org/10.1109/AERO.2012.6187002

[62] Arnold, J. O., Laub, B., Chen, Y.-K., Prabhu, D. K., Bittner, M., and Venkatapathy, E., "Arcjet Testing of Woven Carbon Cloth for Use on Adaptive Deployable Entry Placement Technology," NASA Ames Research Center ARC-E-DAA-TN6341, 2013, https://ntrs.nasa.gov/archive/nasa/casi.ntrs.nasa.gov/20130011056.pdf.

[63] Laub, B., and Venkatapathy, E., "Thermal Protection System Technology and Facility Needs for Demanding Future Planetary Missions," *Planetary Probe Atmospheric Entry and Descent Trajectory Analysis and Science*, ESA Special Publication, Vol. 544, 2004, pp. 239–247, http://adsabs.harvard.edu/abs/2004ESASP.544.239L

[64] Venkatapathy, E., Ellerby, D., Gage, P., Prabhu, D., Gasch, M., Kazemba, C., Kellerman, C., Langston, S., Libben, B., Mahzari, M., et al., "Entry System Technology Readiness for Ice-Giant Probe Missions," *Space Science Reviews*, Vol. 216, No. 2, 2020, pp. 1–21. https://doi.org/10.1007/s11214-020-0638-2

[65] Way, D. W., Powell, R. W., Chen, A., Steltzner, A. D., San Martin, A. M., Burkhart, P. D., and Mendeck, G., "Mars Science Laboratory: Entry, Descent, and Landing System Performance," *2007 IEEE Aerospace Conference*, Inst. of Electrical and Electronics Engineers, New York, March 2007, pp. 1–19. https://doi.org/10.1109/AERO.2007.352821

[66] Venkatapathy, E., Prabhu, D., Allen, G., and Gasch, M., "Thermal Protection System to Enable Ice Giant Aerocapture Mission for Delivering both an Orbiter and an In Situ Probe," *Bulletin of the AAS*, Vol. 53, No. 4, 2021, pp. 1–400. https://doi.org/10.3847/25c2cfeb.0423a253

[67] Hillje, E. R., "Entry Flight Aerodynamics from Apollo Mission AS-202," NASA TN D-4185, Oct. 1967, https://ntrs.nasa.gov/archive/nasa/casi.ntrs.nasa.gov/19670027745.pdf

[68] Justus, C., Duvall, A., and Johnson, D., "Engineering-Level Model Atmospheres for Titan and Neptune," *39th AIAA Joint Propulsion Conference and Exhibit*, AIAA Paper 2003-4803, 2003. https://doi.org/10.2514/6.2003-4803

[69] Justus, C., Duvall, A., and Keller, V., "Atmospheric Models for Aerocapture," *40th AIAA/ASME/SAE/ASEE Joint Propulsion Conference and Exhibit*, AIAA, Reston, VA, 2004, p. 4106. https://doi.org/10.2514/6.2004-3844

[70] Justh, H. L., and Hoffman, J., "Neptune Global Reference Atmospheric Model (Neptune- GRAM): User Guide," NASA Marshall Space Flight Center, NASA/TM–20205001193, 2020.

[71] Duvall, A., Justus, C., and Keller, V., "Global Reference Atmospheric Model (GRAM) Series for Aeroassist Applications," *43rd AIAA Aerospace Sciences Meeting and Exhibit*, AIAA Paper 2005-1239, 2005. https://doi.org/10.2514/6.2005-1239

[72] Seiff, A., Kirk, D. B., Knight, T. C., Mihalov, J. D., Blanchard, R. C., Young, R. E., Schubert, G., Von Zahn, U., Lehmacher, G., Milos, F. S., and Wang, J., "Structure of the Atmosphere of Jupiter: Galileo Probe Measurements," *Science*, Vol. 272, No. 5263, 1996, pp. 844–845. https://doi.org/10.1126/science.272.5263.844

[73] Lindal, G. F., Sweetnam, D., and Eshleman, V., "The Atmosphere of Saturn-An Analysis of the Voyager Radio Occultation Measurements," *Astronomical Journal*, Vol. 90, No. 6, 1985, pp. 1136–1146.

[74] Allen, G. A., Jr., Marley, M. S., and Agrawal, P., "Uranus Atmospheric Model for Engineering Application," *Workshop on the Study of the Ice Giant Planets*, Vol. 1798, Johns Hopkins Univ., Applied Physics Lab., Laurel, MD, 2014, p. 2001, https://www.hou.usra.edu/meetings/icegiants2014/presentations/Day_2/Allen_2001.pdf.

[75] Longuski, J. M., and Williams, S. N., "Automated Design of Gravity-Assist Trajectories to Mars and the Outer Planets," *Celestial Mechanics and Dynamical Astronomy*, Vol. 52, No. 3, 1991, pp. 207–220. https://doi.org/10.1007/BF00048484

[76] Yam, C. H., Davis, D. C., Longuski, J. M., Howell, K. C., and Buffington, B., "Saturn Impact Trajectories for Cassini End-of-Mission," *Journal of Spacecraft and Rockets*, Vol. 46, No. 2, 2009, pp. 353–364. https://doi.org/10.2514/1.38760

[77] Hughes, K. M., "Gravity-Assist Trajectories to Venus, Mars, and the Ice Giants: Mission Design with Human and Robotic Applications," Ph.D. Thesis, Purdue Univ., West Lafayette, IN, 2016.

[78] Mansell, J., Kolencherry, N., Hughes, K., Arora, A., Chye, H., Coleman, K., Elliott, J., Fulton, S., Hobar, N., Libben, B., Lu, Y., Millane, J., Mudek, A., Podesta, L., Pouplin, J., Shibata, E., Smith, G., Tackett, B., Ukai, T., Witsberger, P., and Saikia, S., "Oceanus: A Multi-Spacecraft Flagship Mission Concept to Explore Saturn and Uranus," *Advances in Space Research*, Vol. 59, No. 9, 2017, pp. 2407–2433. https://doi.org/10.1016/j.asr.2017.02.012

[79] Chapman, D. M. F., "Recurrent Phenomena of Venus and the Venus/Earth Orbital Resonance," *Journal of the Royal Astronomical Society of Canada*, Vol. 80, No. 6, 1986, pp. 336–343, http://adsabs.harvard.edu/abs/1986JRASC.80.336C.

[80] Harrison, E., and Pritchard, E., "Lifting Entry Unmanned Viking Class Mars Landers," NASA TN D-5828, 1970.

[81] Murphy, K., Brauckmann, G., Bell, J., Rhode, M., Owens, D. B., Wilson, T., Bibb, K., Chan, D., and Walker, E., "Orion Crew Module Aerodynamic Testing," *29th AIAA Applied Aerodynamics Conference*, AIAA Paper 2011-3502, 2011. https://doi.org/10.2514/6.2011-3502

[82] Malphrus, B. K., Freeman, A., Staehle, R., Klesh, A. T., and Walker, R., "Interplanetary CubeSat Missions," *Cubesat Handbook*, Elsevier, London, U.K., 2021, pp. 85–121. https://doi.org/10.1016/B978-0-12-817884-3.00004-7

[83] Hassett, R., "Design Integration of Aerocapture and Aeromaneuver Vehicles for a Mars Sample Return Mission," *21st Structures, Structural Dynamics, and Materials Conference*, AIAA Paper 1980-0728, 1980. https://doi.org/10.2514/6.1980-728

[84] Lyne, J. E., "Physiologically Constrained Aerocapture for Manned Mars Missions," NASA TM-103954, 1992.

[85] Ramsey, P., and Lyne, J. E., "Enceladus Mission Architecture Using Titan Aerogravity Assist for Orbital Capture About Saturn," *Journal of Spacecraft and Rockets*, Vol. 45, No. 3, 2008, pp. 635–638. https://doi.org/10.2514/1.31362

[86] Martin-Mur, T. J., Abraham, D. S., Berry, D., Bhaskaran, S., Cesarone, R. J., and Wood, L., "The JPL Roadmap for Deep Space Navigation," American Astronautical Society, AAS Paper 06-223, Springfield, VA, 2006.

[87] Moore, J., "Scientific Goals for Exploration of the Outer Solar System," Vol. 28, TR OPAG-Report-Draft-Aug-2019, Lunar and Planetary Inst., Houston, TX, Aug. 2019, https://www.lpi.usra.edu/opag/goals-08-28-19.pdf.

[88] Ghail, R., Wilson, C., Widemann, T., Bruzzone, L., Dumoulin, C., Helbert, J., Herrick, R., Marcq, E., Mason, P., Rosenblatt, P., Vandaele, A. C., and Burtz, L.-J., "EnVision: Understanding Why Our Most Earth-like Neighbour is so Different," ArXiv e-prints, 2017, https://arxiv.org/abs/1703.09010.

[89] "Announcement of Opportunity (AO) to International Science Community for Space-Based Experiments to Study Venus," TR, Indian Space Research Organization, Bangalore, India, 2018, https://www.isro.gov.in/sites/default/files/ao venus.pdf.

[90] Venkatapathy, E., Ellerby, D., Gage, P., Dinesh, P., Gasch, M., Cole, K., Kellerman, C., Langston, S., Libben, B., Milad, M., Milos, F., Murphy, A., Nishioka, O., Peterson, K., Poteet, C., Splinter, S., Stackpoole, M., Williams, J., and Young, Z., "Entry System Technology Readiness for Ice-Giant Probe Missions," *Space Science Reviews*, Vol. 216, No. 2, 2020, pp. 1–21. https://doi.org/10.1007/s11214-020-0638-2

[91] Rollock, A. E., and Braun, R. D., "Analysis of Hypersonic Tip-Off Rates for Venus Aerocapture," *AIAA Scitech 2020 Forum*, AIAA Paper 2020-1739, 2020. https://doi.org/10.2514/6.2020-1739

[92] McClary, M., and Putnam, Z. R., "Assessment of Hypersonic Separation Dynamics for Drag Modulation Systems at Mars," *AIAA Scitech 2021 Forum*, AIAA Paper 2021-1063, 2021. https://doi.org/10.2514/6.2021-1063

[93] Albert, S. W., and Braun, R. D., "Conceptual Development of AeroDrop: Aerocapture and Direct Entry for Two Spacecraft on a Common Approach Trajectory," *AIAA Scitech 2020 Forum*, AIAA Paper 2020-1737, 2020. https://doi.org/10.2514/6.2020-1737

[94] Justh, H. L., "Overview of Global Reference Atmospheric Model (GRAM) Upgrades," *15th International Planetary Probe Workshop*, Univ. of Colorado, Boulder, 2018.

G. E. Palmer
Associate Editor